COIL SENSITIVITY MAP CALCULATION USING BIOT-SAVART LAW AT 3
TESLA AND PARALLEL IMAGING IN MRI

A THESIS SUBMITTED TO
THE GRADUATE SCHOOL OF NATURAL AND APPLIED SCIENCES
OF
MIDDLE EAST TECHNICAL UNIVERSITY

BY

YUNUS EMRE ESİN

IN PARTIAL FULFILLMENT OF THE REQUIREMENTS
FOR
THE DEGREE OF DOCTOR OF PHILOSOPHY
IN
COMPUTER ENGINEERING

MARCH 2017

Approval of the thesis:

COIL SENSITIVITY MAP CALCULATION USING BIOT-SAVART LAW AT 3 TESLA AND PARALLEL IMAGING IN MRI

submitted by **YUNUS EMRE ESİN** in partial fulfillment of the requirements for the degree of **Doctor of Philosophy in Computer Engineering Department, Middle East Technical University** by,

Prof. Dr. Gülbin Dural Ünver
Dean, Graduate School of **Natural and Applied Sciences**   ⎯⎯⎯⎯⎯⎯

Prof. Dr. Adnan Yazıcı
Head of Department, **Computer Engineering**   ⎯⎯⎯⎯⎯⎯

Prof. Dr. Ferda Nur Alpaslan
Supervisor, **Computer Engineering Department, METU**   ⎯⎯⎯⎯⎯⎯

Examining Committee Members:

Prof. Dr. Mehmet Resit Tolun
Electrical & Electronics Engineering Department, Aksaray Uni.   ⎯⎯⎯⎯⎯⎯

Prof. Dr. Ferda Nur Alpaslan
Computer Engineering Department, METU   ⎯⎯⎯⎯⎯⎯

Assoc. Prof. Dr. Ahmet Oğuz Akyüz
Computer Engineering Department, METU   ⎯⎯⎯⎯⎯⎯

Assist. Prof. Dr. Çiğdem Turhan
Computer Engineering Department, Atılım Uni.   ⎯⎯⎯⎯⎯⎯

Assist. Prof. Dr. Şeyda Ertekin
Computer Engineering Department, METU   ⎯⎯⎯⎯⎯⎯

Date: ⎯⎯⎯⎯⎯⎯

I hereby declare that all information in this document has been obtained and presented in accordance with academic rules and ethical conduct. I also declare that, as required by these rules and conduct, I have fully cited and referenced all material and results that are not original to this work.

Name, Last Name: YUNUS EMRE ESİN

Signature   :

ABSTRACT

COIL SENSITIVITY MAP CALCULATION USING BIOT-SAVART LAW AT 3 TESLA AND PARALLEL IMAGING IN MRI

Esin, Yunus Emre

Ph.D., Department of Computer Engineering

Supervisor   : Prof. Dr. Ferda Nur Alpaslan

March 2017, 82 pages

Coil spatial sensitivity map is considered as one of the most valuable data used in parallel magnetic resonance imaging (MRI) reconstruction. In this study, a novel sensitivity map extraction method is introduced for phased-array coils. Proposed technique uses Biot-Savart law with coil shape information and low-resolution phase image data to form sensitivity maps. The performance of this method has been tested in the parallel image reconstruction task using sensitivity encoding technique.

In MRI, coil sensitivity maps are complex-valued data that are typically represented with two components: phase and magnitude. In the proposed method, the phase information is retrieved from low-resolution central k-space signal data and the magnitude information is calculated using Biot-Savart law. Under the quasi-static assumption and using the duality principle, the spatial sensitivity maps of a head coil was computed for using parallel MRI reconstruction.

In our experiments, volunteer and phantom scans were obtained using a 32-channel

head coil and full field of view images were reconstructed using the proposed method. Experiments show that the resulting image qualities are higher than the ones obtained by the existing methods that use sensitivity maps calculated only from low-resolution image data. Moreover, several simulations were conducted using an electromagnetic simulation software tool to theoretically prove the success of the proposed technique. These simulation results indicate that the success of our method depends heavily on the size of the coil elements.

Briefly, a new method for calculation of coil sensitivity is introduced which increases the image quality and homogeneity while reducing the artifacts.

Keywords: MRI, coil sensitivity profiles, parallel MRI, phased array coil, MRI in-homogeneity correction

ÖZ

BİOT-SAVART YASASI KULLANARAK BOBİN HASSASLIK HARİTALARININ HESAPLANMASI VE MRG'DE PARALEL GÖRÜNTÜLEME

Esin, Yunus Emre

Doktora, Bilgisayar Mühendisliği Bölümü

Tez Yöneticisi   : Prof. Dr. Ferda Nur Alpaslan

Mart 2017 , 82 sayfa

Uzamsal anten duyarlılık haritası, paralel manyetik rezonans görüntüleme (MRG) tekniğinde kullanılan en değerli veri olarak kabul edilir. Bu çalışmada, faz dizili bobinler için yeni bir duyarlılık haritası çıkarma yöntemi önerildi. Önerilen teknik hassaslık haritasını oluşturmak için Biot-Savart yasası ile bobin şekil bilgisini ve düşük çözünürlüklü faz görüntü verisini kullanmaktadır. Bu yöntemin performansı paralel imge oluşturma görevinde hassaslık kodlama tekniği kullanılarak test edildi.

MRG'de, bobin duyarlılık haritaları tipik olarak iki bileşen (faz ve miktar olarak) ile temsil edilen karmaşık sayılardan oluşan bir veridir. Önerilen yöntemde, faz bilgisi düşük çözünürlüklü merkezi k-uzayı sinyal verisinden çıkarılır ve büyüklük bilgisi ise Biot-Savart yasası kullanılarak hesaplanmaktadır. Paralel MRG yapımı için, yarı-statik varsayımı altında ve dualite prensibi kullanılarak, faz dizili bir kafa koilinin uzamsal duyarlılık haritaları hesaplanmıştır.

Deneylerimizde, 32 kanallı bir kafa bobini kullanılarak gönüllü ve fantom taramaları elde edildi ve tam görüş alanı görüntüleri önerilen yöntem kullanılarak oluşturuldu. Deneyler gösteriyor ki ortaya çıkan görüntü kaliteleri, sadece düşük çözünürlüklü imge verilerinden hesaplanan duyarlılık haritaları kullanan mevcut yöntemlere göre daha yüksektir. Dahası, önerilen tekniğin başarımını ispatlamak için bir elektromanyetik simülasyon yazılım aracı kullanarak çeşitli simülasyonlar yapılmıştır. Bu simülasyon sonuçları gösteriyor ki bizim yöntemimizin başarımı ağırlıklı olarak koil elemanlarının büyüklüğüne bağlıdır.

Kısaca, görüntü kalitesini ve homojenitesini artırırken artifaktları azaltan, yeni bir koil duyarlılığı hesaplamak yöntemi önerilmiştir.

Anahtar Kelimeler: MRG, koil duyarlılık profilleri, paralel MRG, faz dizili koil, MRG homojensizlik düzeltimi

To my family and parents

ACKNOWLEDGMENTS

TABLE OF CONTENTS

LIST OF TABLES

TABLES

LIST OF FIGURES

FIGURES

xvi

LIST OF ABBREVIATIONS

2D	Two-dimensional space
3D	Three-dimensional space
CPU	Central Processing Unit
CT	Computed Tomography
DICOM	Digital Imaging and Communications in Medicine
MR	Magnetic Resonance
MRI	Magnetic Resonance Imaging
fMRI	Functional MRI
FOV	Field of view
GPU	Graphics Processing Unit
GRAPPA	**G**ene**R**alized **A**utocalibrating **P**artially **P**arallel **A**cquisitions
RF	Radio Frequency
PET	Positron Emission Tomography
PILS	Partially Parallel Imaging with Localized Sensitivities
pMRI	Parallel Imaging in MRI
SAR	Specific Absorption Rate
SENSE	**Sens**itivity **E**ncoding for Fast MRI
SMASH	**Si****M**ultaneous **A**cquisition of **S**patial **H**armonics
SNR	Signal to Noise Ratio
UMRAM	Ulusal Manyetik Rezonans Araştırma Merkezi (National Magnetic Resonance Research Center)

CHAPTER 1

INTRODUCTION

In this doctoral study a novel technique for the construction of better coil spatial sensitivity maps is introduced in order to improve the quality of the images produced from the MRI scanners. **Parallel image reconstruction** and **coil inhomogeneity correction** in MRI were selected for the application area of our technique. This technique uses coil internal shape information and Biot-Savart Law. It is tested at magnetic field strength of 3 Tesla and can be used in lower magnetic fields as well.

1.1 Motivation

There is no doubt that health is one of the greatest assets of any living creature. Therefore, any improvement in health care has a great importance for us. This is the very first motivation that we had while starting this study.

Today, there exists a wide range of medical imaging systems. Each has its own motivation area in terms of diagnosis. Some of the well-known imaging systems are: X-Ray, CT, Tomography, MRI, Ultrasound, Endoscopy, and Thermography. There are also some others which are not familiar to most of us since either their usage areas are very limited or they are not that useful.

A list of popular medical imaging devices and their descriptions are provided in Table 1.1. Among all these systems, currently, MRI is the most advanced and flexible tool in terms of imaging capabilities in medicine. It can provide cross sectional images of the body internals (organs, tissues and structures) in any orientation, while the others

Table1.1: List of Medical Imaging Devices

Medical Imaging Device	Description
Magnetic Resonance Imaging (MRI)	The technique which make use of magnetic fields and radio frequencies to make pictures of tissues and structures inside the body ([2]).
Nuclear medicine	In this technique, radioactive substances are taken from the patient and the radiation emitted from these substances are captured from external detectors. The signal data is then transformed into images ([3]).
Ultrasound	Sounds with a frequency of higher than the upper audible limit (above 20,000 Hz) of human hearing is used for visualizing the tissues and organs ([4, 5]).
Elastography	Medical imaging technique which aims to find the elastic properties of soft tissues. The main working principle of this technique is that: it creates a distortion in the tissue and then observe and analyze the response ([6]).
Tactile imaging	Similar to the Elastography, the main aim is to measure the elasticity, hardness and stiffness of the corresponding tissues ([7]).
Photoacoustic imaging	In this technique laser pulses are delivered into the tissues and some of the energy is absorbed which produces heat. The heat generates ultrasonic waves which are detected from the sensors and then converted into images ([8]).
Thermography	Thermal cameras are used to detect the radiation in the long-infrared range of the electromagnetic spectrum. In this technique the thermal changes over the body is detected which indicates the metabolism rate and shows the signs of some of the illnesses([9, 10, 11, 12, 13]).
Tomography	Tomography aims to image a single plane or slice of an object. Either conventionally or computationaly the internal structures of the human body can be visualized using this technique. Most of the time ionizing radiation (X-Rays) are used for determining the internals of the subject ([14, 15, 16]).
Echocardiography	This technique uses either 2D or 3D doppler ultrasond to visuealize the hearth ([17]).
Functional near-infrared spectroscopy	For collecting information about the functional propoerties of neurons in this technique near-infrared spectroscopy is used ([18, 19]).

cannot. According to [20], MRI provides the most important diagnostic information which cannot be obtained from any other medical imaging techniques. In addition, MRI examinations do not involve the use of ionizing radiation and therefore, MRI is relatively safe when compared to the rival medical imaging devices such as Tomography and X-Ray. Moreover, as people become conscious about the side effects of the medical imaging devices, they hesitate over the usage of these system. Fortunately, MRI technique is not one of these techniques and in the future, its usage will continue to increase. A detailed analysis of MR machine and its effects on human body is given in [21]. Briefly, MRI is not only one of the safest technique, but also the most advanced one in terms of imaging capabilities. All these make MRI very important.

MR is a medical imaging device which uses the magnetic field and radio waves to create internal pictures of the body ([22, 23]). [24] and [25] give details of MR machine and MRI. A sample MR machine, which is the one that we used for this study, is given in Figure 1.1.

The basic working principle of an MR machine is as follows:

- MR creates a strong magnetic field around the imaged body and it uses the protons (hydrogen atoms) inside the tissues to create signals.

- First an RF energy is given to the imaging body temporarily in specific conditions (for example at a proper resonance frequency).

- Then the exited hydrogen atoms emit the given energy as a radio frequency signal which is received and measured from coils.

- Finally, this information is then processed and converted into MR images which are used for medical purposes.

A detailed explanation of how an MR machine works and the operational modes that are useful for clinical applications are explained in [26, 27].

Currently MRI technique is used in investigation and staging of a wide range of diseases. Using MR machines, almost all systems of our bodies (such as central nervous system, cardiovascular system, musculoskeletal system, liver and the gastrointestinal

system) can be visualized for detailed analysis of possible illnesses. To illustrate, for the cancer patients, using MRI, diagnosis, staging, and follow-up of the tumors can be possible. Moreover, with functional MRI (fMRI), brain responses for the external stimuli can be investigated [28]. Furthermore, with MRI spectroscopy [29] biochemical information of the tissues can be obtained and its application areas are given in [30].

There are lots of different usage areas of MRI. Some of the possible reasons for the need of an MRI examination is given in [31]. In short, MRI has a wide range of application areas in medicine and it is one of the most advanced medical imaging system in terms of the image quality it provides and the body parts it can visualize.
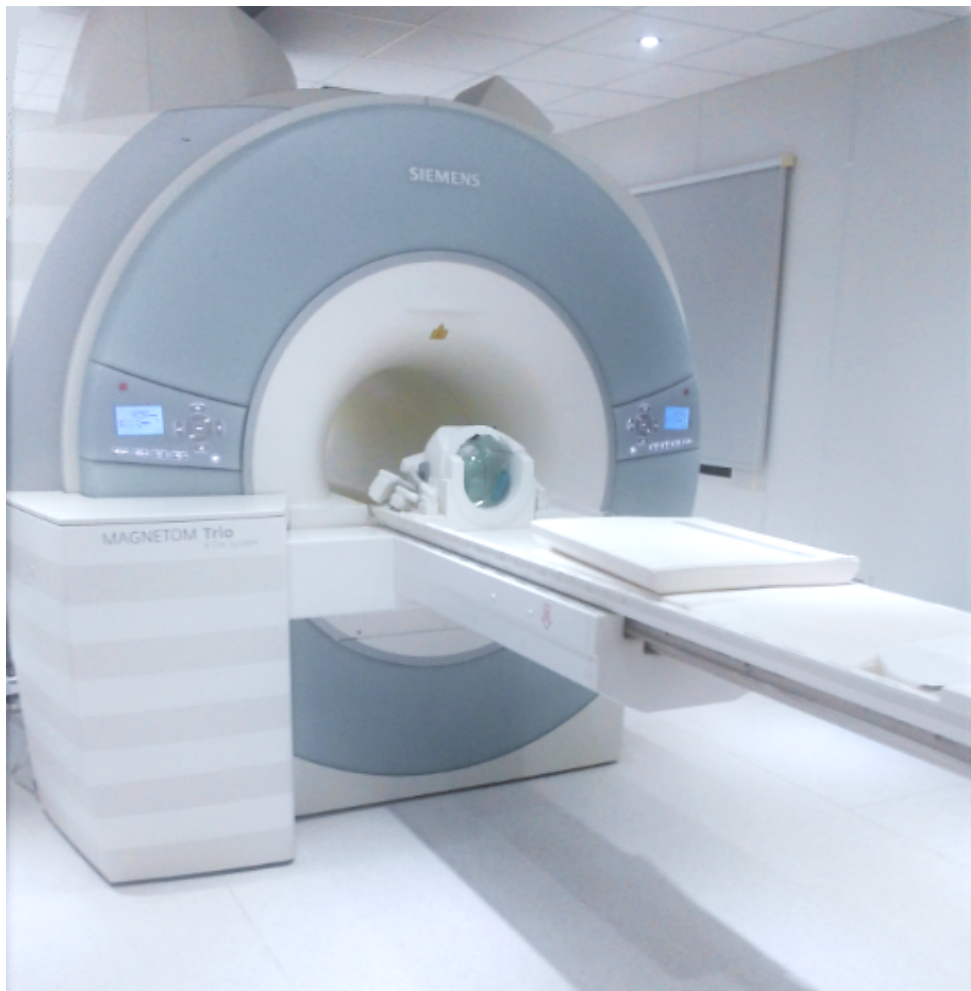
Figure 1.1: MR machine used in this study

1.1.1 Computer Engineering and MRI

Even though Physics and Electrical & Electronics Engineering are the two major disciplines that are interested in the improvement of MRI technique, Computer Engineering can also provide significant contributions to this research area. Since the MR machine is a kind of imaging device, some of the image and signal processing techniques available in computer engineering can be used for the construction of better quality images. In addition, such methods can be further improved or new techniques can be developed for the enhancement of MRI to increase the quality of the images produced.

1.2 Problem Definition and Scope of the Thesis

An MRI examination can take several minutes to hours depending on the scan configuration, number of slices, size of the area being scanned and the specifications of the machine. In addition, depending on the patient's condition, long scan duration can cause negative effects on the body of patients both mentally and physically. [32, 33] mentioned about health, biological and physiological effects of MRI on human body. [34] listed the safety issues regarding to MRI examinations. According to these studies exposure duration and the magnetic field strength are the two important factors that may have negative side effects on human body. Therefore, the techniques for decreasing the exposure duration is currently the focus of several scientists working in the research area of MRI.

Unfortunately, current MRI machines have already reached their physical operation speed limits and scientists have been looking for alternative ways. In order to further increase the MRI examinations, in the last decades, parallel imaging methods in MRI have been developed to solve the speed problem. Using these techniques, the speed of acquisitions can be increased not just physically but also computationally. Therefore, they are independent from the physical capabilities of MR machines.

The parallel imaging techniques in MRI world are called as parallel imaging in MRI (pMRI). By applying pMRI methods, imaging speed of an MR examination can be

increased in several folds [35]. Until now, scientists have developed a large number of pMRI methods. However, there is still much to do in this area, and therefore, pMRI is still one of the hot topics in MRI research world.
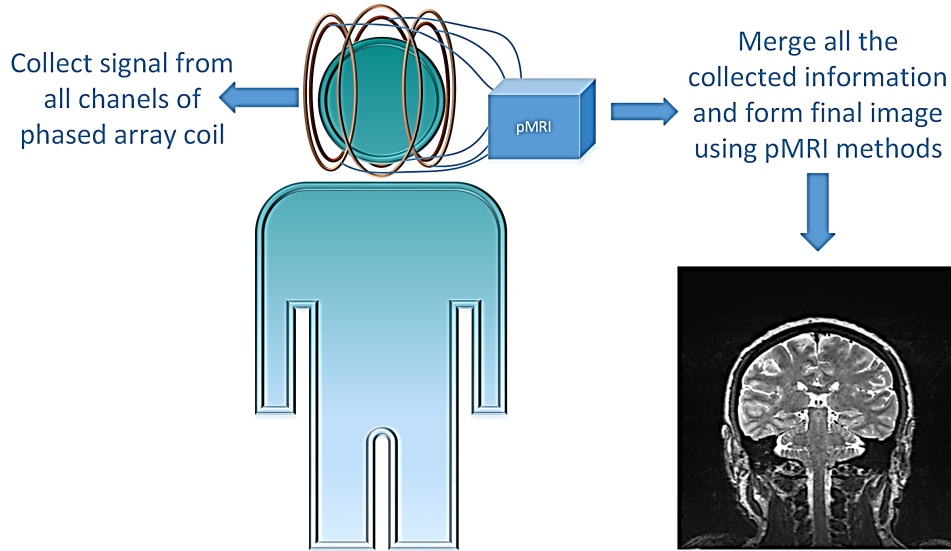
Figure 1.2: pMRI with phased-array surface coil. In the figure, human represents the patient, rings represent the coil channels and the cube represents the pMRI method processor which collects the information from all channels which are merged to form the reconstructed image.

The main idea behind pMRI is that, instead of collecting signal information from one channel of a phased-array coil in a long period of time, the data is collected from all channels in a short amount of time simultaneously. Then, by using parallel imaging techniques, the collected information is merged to construct the final images. Therefore, in order to apply pMRI, one of the most important prerequisite is the usage of multi-channel receiver coils in the MR examinations. Figure 1.2 illustrates how pMRI technique is used with a phased-array surface coil.

As expected, in the last decades, scientists concentrated on the development of phased-array coil systems, besides the single channel coils. Currently, phased-array coils are becoming popular and they are used in MR machines for several purposes in many hospitals. In addition, as stated in [36], using phased-array coils cannot only decrease the time needed for MRI examinations but also can cover a wider area in one scan. Moreover, it increases the signal to noise ratio (SNR), and thus, image quality can be improved significantly.

1.2.1 Parallel imaging in MRI

According to [37], parallel MRI works by acquiring a reduced amount of signal data with an array of receiver coils. Since the collected data is decreased by skipping some of the lines (i.e. under-sampling) in signal space, the scan speed is increased accordingly. However, the under-sampling leads to aliased/folded-over images when the signal space is transformed into the image space. Afterwards, parallel imaging algorithms can be used for unfolding the overlapped images and this process aims to reconstruct artifact-free, full versions' of the images. Some of the parallel imaging techniques reconstruct the images in image domain (such as SENSE [38]), but some others do this operation in the signal domain (such as GRAPPA [39]).

Parallel MRI techniques consist of several steps of algorithms and their main aim is to combine information coming from each coil channel of a phased-array coil to come up with a final image. Even though there are significant differences among existing parallel MRI methods, all use the same crucial data: **coil spatial sensitivity information**. This data is mainly used for unfolding the overlapped images because of the under-sampled k-space (Figure 1.3) [40, 41] data. The information inside the overlapped/merged pixels are separated according to the coil sensitivity ratios of the actual pixel positions in the unfolded image.

Coil sensitivity is a complex-valued data and its value at a point in the space is the coil response at that location. Depending on various reasons such as: the coil shape, location and the imaging objects internal properties, sensitivity value of a coil at a point in the imaging space changes. Therefore, construction of images (without any post process) by using solely the signal data which is collected by coil channels can cause non-uniform images.

In the large body coils which are installed in the magnet of MRI machine spatial sensitivities are almost uniform in lower magnetic fields ($B_0 \leq 1.5$), but in surface coils, and especially in small-sized coils, sensitivities have different non-homogeneous characteristics. In addition, in case of coils with complicated internal shapes and higher magnetic fields ($B_0 > 1.5\ Tesla$) of the MR machines, the in-homogeneity becomes a serious problem. This issue can cause significant artifacts in the images depending
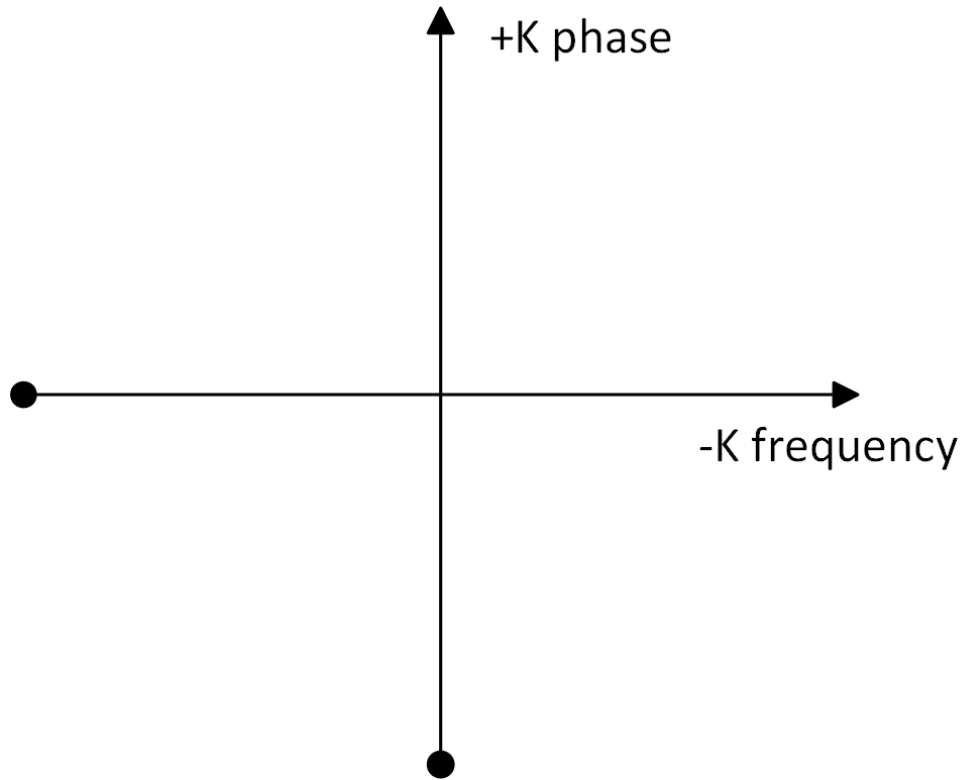
Figure 1.3: k-space. The raw MR signal data is held in this coordinate system. Horizontal axis is for frequency of the signal and vertical axis is used for the phase information of the signal data.

on the sensitivity variations over the imaging region. These artifacts are very common and can decrease the quality of the images remarkably, especially in the ones which are reconstructed by parallel MRI techniques.

1.2.2 MRI Image In-homogeneity Artifact

In-homogeneity problem is the slow intensity variations on the same tissue image and it is independent from the body internals. This problem can be caused from several reasons such as: RF in-homogeneity, static field non-uniformity or sensitivity variations of the coils. In this study, we focused on the RF in-homogeneity problem which is caused from the coil sensitivity variations. If the coil spatial sensitivities are found precisely in the imaging space, this problem in the images can be eliminated by applying normalization operations using spatial coil sensitivities and the collected signals. That is, the signal magnitude at all positions in an imaging space is divided

by the corresponding sensitivity values to normalize the signal at all locations. Thus, homogeneous and better quality images can be obtained.

In-homogeneity artifacts in the MRI images become more apparent when surface coils are used, especially in higher fields ($B_0 \geq 3$). In such cases, these artifacts cause trouble especially in image segmentation, registration and parallel image reconstruction processes. Therefore, even if there is no parallelization in the MRI scans, finding the coil spatial sensitivities will have great importance on the correction of coil in-homogeneities.

Figure 1.4 illustrates an MRI image of a uniform phantom. Normally the imaged object should have a homogeneous intensity in all over the regions (a more uniform image is formed by the MR machine is shown in Figure 1.5) however, because of the coil spatial sensitivity variations, phantom image doesn't have a uniform color.
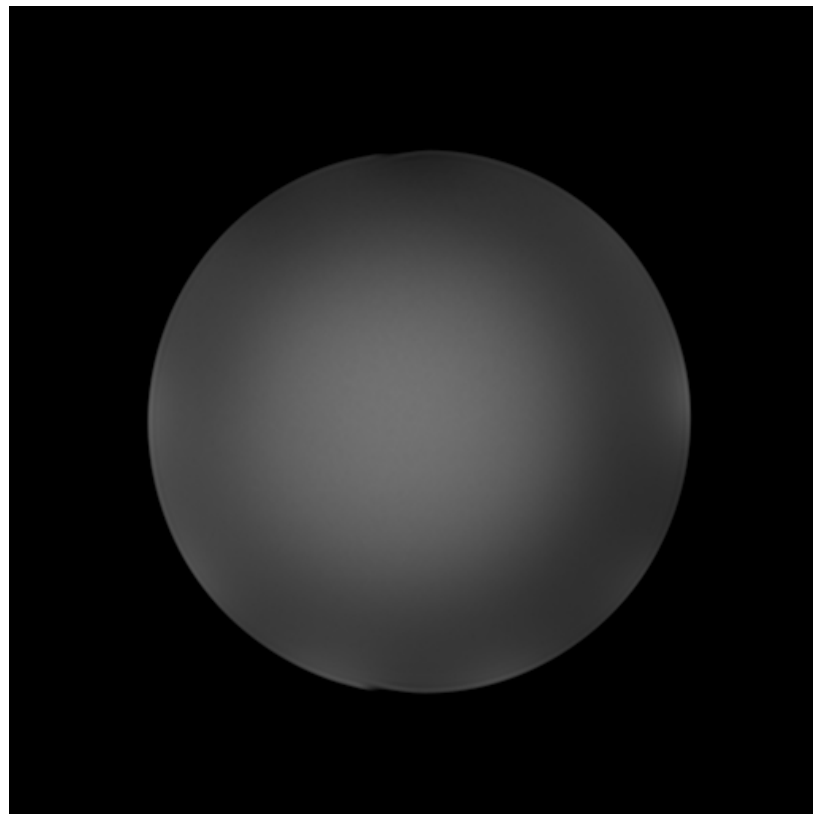
Figure 1.4: In-homogeneity caused from coil sensitivity variations.
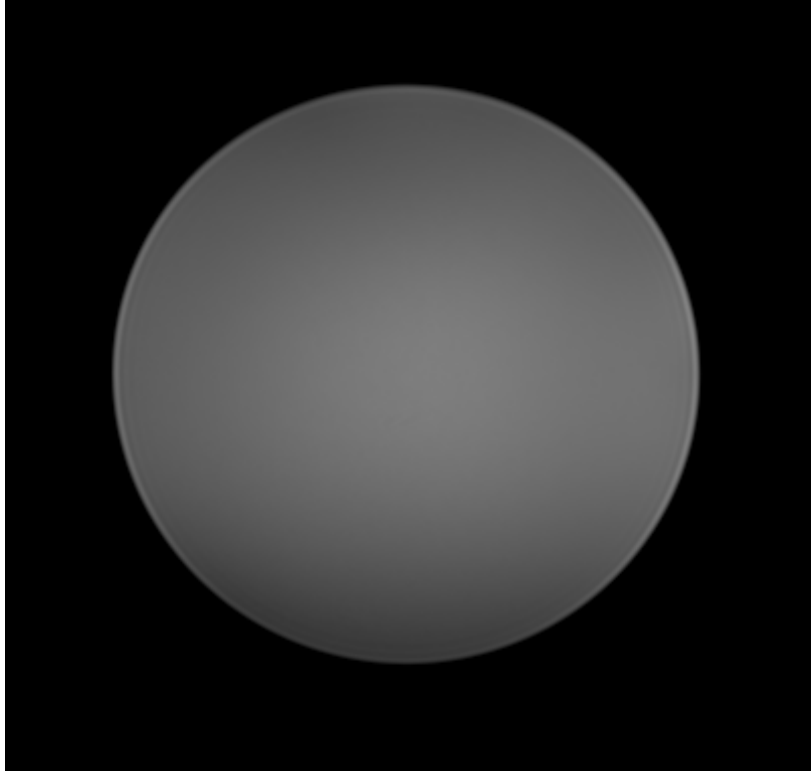
Figure 1.5: Homogeneous phantom image.

1.2.3 Focus of the study

In this study, MR coil sensitivities are found using their 3D internal wire shape information. In most of the previous studies, the sensitivities are found using low resolution reference scan data. In this study, this data and the coil shape information are combined to provide much better maps instead. Therefore, the focus was on the combination of scan data and physical shape data.

The coil sensitivities of a commercial phased-array head coil [1] is found and the success of the method is proven by comparing the results with those obtained by the well-known parallel MRI methods. In addition, the computed sensitivity information is used to correct the coil intensity in-homogeneities in the images taken using this head coil.

Basic flow of the processes in the proposed method is shown in the figure 1.6). First the coil sensitivities are found using the 3D geometry information of the coil channels then the MRI examination is performed. If the scan is in accelerated mode the next

step is finding the combined coil sensitivity maps and applying parallel image reconstruction techniques. However, if the scan is in normal mode the calculated sensitivity maps are used for intensity inhomogeneity correction. In each case higher quality images are produced when compared to the machines' outputs. Once the sensitivities are found using the coil shapes it can be used in future scans. Details of each step is explained in chapter 4.
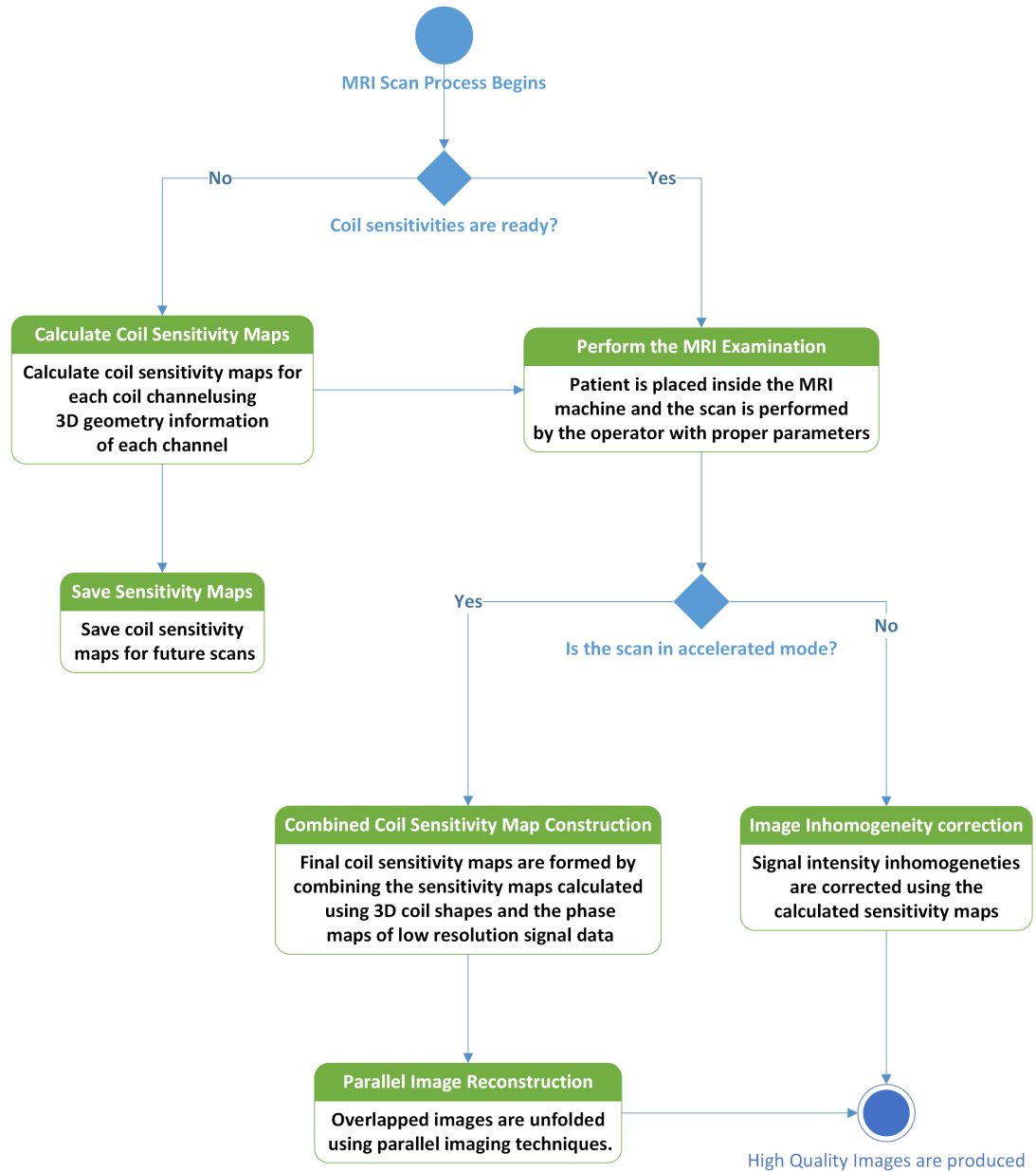
Figure 1.6: Process flow chart of the proposed method.

1.3 Contributions of the Thesis

In almost all parallel MRI methods, coil spatial sensitivity information is found from the estimations using low-resolution signal data in each scan on-the-fly (i.e. within the MR examination). In non-parallel scans, coil sensitivities can also be found by similar estimation processes and used for fixing intensity variations during the image construction processes.

In this study, a new coil spatial sensitivity map extraction method is introduced. This technique has two major steps. The first step is computing the spatial sensitivities using coil shape information and Biot-Savart law. The second step is combining the found map with the one estimated from low-resolution scan data. Thus, the map found from two different processes are combined and, therefore, a better estimated map information is obtained. Currently, this method was proposed for spatially fixed phased-array coils but it can be extended to many coils after applying a pre-processing. In addition, the first step of our method is processed once but it can be applied to the scan data in every MRI examination as many times needed.

1.4 Outline of the Thesis

In Chapter 2, related studies which are found in the literature survey are given. In this chapter not only the studies, but also their advantages and disadvantages are discussed. In Chapter 3, we present the theory behind this study. Chapter 4 explains our methodology and gives several illustrative samples. To show the success and effectiveness of our method, several experimental setups were prepared which are explained in Chapter 5. In Chapter 6, the results of our method are discussed in detail and compared with the outcome of the existing similar studies in the literature. Finally, in Chapter 7, the conclusion gives the final remarks, proposing possible related future studies.

CHAPTER 2

LITERATURE SURVEY

This thesis study concentrates on both **parallel imaging** and **intensity in-homogeneity problem** of gray-scale images in MRI. This chapter analyzes the related studies in the literature in two sections. They are:

- Parallel Imaging in MRI

- Intensity In-homogeneity Correction in MRI.

2.1 Parallel Imaging in MRI

There are several improvement areas of MRI technology. Among all these areas, the most important ones are related to **image quality** and **scan acquisition speed**. There are lots of studies in the literature aiming to make improvements on these areas. While some of the studies concentrate on acceleration of the MRI scans, some others focus on the improvement of image qualities, or both. Scientists made contributions in these areas with providing new hardware designs and developing new software based solutions in MRI scanners.

Before the studies [42] and [43], scientists made various contributions on MRI scanners to speed up the scans by using single receiver coils. However, due to the physical limitations, MRI scanners have already closely reached their operational speed limits. Since the speed improvements in single coil strategy has reached its limits, multiple receiver coils have recently been introduced. Some of the earliest studies which brought out the usage of multiple receiver coils are [42] and [43]. Their main

idea was, instead of receiving signals from a single receiver coil, the combination of information gathered from multiple coils could increase the quality of the images. This idea has been successful, so that, scientists working in this area focused mainly on the usage of multiple receiver coils in MRI examinations and until now they have made lots of improvements in the area of MRI.

Usage of multiple antennas is specific to MRI technology. Actually, there are a wide range of usage areas. In the literature this technique is called as **phased array**. Nuclear magnetic resonance imaging [44], radar technology [45], antenna theory [46], optics [47], radio-frequency identification (RFID) [48], ultrasound technology [49], space industry, military ... etc. are all usage areas of phased array methodology.

One of the greatest techniques came along with the usage of multiple coils simultaneously to speed up MRI image acquisition process. By combining the signal collected from each channel of a phased array coil, the speed can be increased significantly. In addition, usage of multiple coils simultaneously provides collection of more signals and coverage of wider areas in a single MRI scan besides the speed up. This technique is called as **parallel imaging in MRI (pMRI)**. It is a combination of hardware and software based solutions.

Parallel imaging methodology contains all of the data combination techniques where the data is collected from different kind of sources in MRI. [35] and [50] give the basics of parallel imaging techniques in MRI. Basically, pMRI methods reconstruct the images by merging the signal information collected from each coil in a multi-coil receiver system. In the merge operation, spatial sensitivity information of each coil is used to form the final images. In normal (not accelerated) image acquisitions coil sensitivities define the mixing ratio of each channel's signal data. But in accelerated mode, coil sensitivities are also used for unfolding the overlapped images. In accelerated modes, the acceleration in the scan comes from the reduced acquisition times which requires less signal data in an MRI examination. The missing information, because of the accelerated scan, is then compensated from the coil spatial sensitivities. Therefore, in pMRI, finding the coil sensitivity map information is crucial.

Some of the earliest studies on pMRI are [51], [44], [52] and [53]. Until 1997, the studies on pMRI were not put into use on commercial MRI scanners. However, with

the study [54], pMRI became available on MRI machines. Currently, four of the well-known pMRI techniques, which are also commercially available for clinical use, are SMASH [54], SENSE [38], PILS [55] and GRAPPA [39]. A detailed analysis of these four methods are given in [56]. In addition, among all, **SENSE** and **GRAPPA** are the two most important (state-of-art) pMRI methods.

2.1.1 Parallel MRI in Image and Frequency Domains

In the literature, there are hundreds of studies about pMRI. Even though each method has its own way of reconstruction, all of the studies can be categorized in three main groups. These groups are as following:

- Image domain pMRI methods

- Frequency domain pMRI methods

- pMRI methods on both image and frequency domains

In the following subsections, each of these category studies are examined.

2.1.1.1 Image Domain pMRI Methods

Parallel imaging methods in this category solves the overlapping problem caused by accelerated scans in image domain. Therefore, the first step is to transform the signal data into image data. This transformation is done by applying Fourier transformation.

In image domain pMRI techniques, image is handled as a collection of pixels. In the overlapped regions, pixels contain information from more than one region of the imaging subject. Figure 2.1a shows a folded over image and the pixels in the overlapped regions illustrate the ones which contain cumulative information of the corresponding 2 pixels in the unfolded version of the same image as in Figure 2.1b. Scientists have developed several approaches to solve the overlap problem and their main aim is to separate the information in each pixel containing the accumulated data from different parts of the imaged subject and, thus, the final unfolded images are generated.

The best samples of image domain methods are SENSE and PILS. There are also other studies which concentrated on the improvement of these two methods. Some of the studies that concentrated on image domain solutions are [57], [58], [59], [60], [61], [62] and [63].

2.1.1.2 Frequency Domain pMRI Methods

Contrary to the image domain methods, this category works on a signal domain. In accelerated scans, some of the lines in k-space (some of the phase encoding signal lines) are missed, which is the main reason behind the speed-up. Frequency domain parallel MRI methods aim to estimate these missing lines using the collected ones.

In frequency domain category, methods GRAPPA and SMASH are the well-known ones. There are also several other methods in this category. For example, studies: [64], [65] and [66] made improvements on SMASH and [67], [68], [69] and [70] made improvements on the GRAPPA method.

2.1.1.3 pMRI Methods on both Image and Frequency domains

While all the previous methods are separated according to the domains which they work on, in the recent study [71] (ESPIRiT), the benefits of the famous two pMRI methods (SENSE and GRAPPA) are combined.

2.1.2 Coil Sensitivity Extraction Approaches

As the studies [72] and [73] stated, in a parallel image reconstruction process, the most important step is the calculation of coil sensitivity maps. While studies have been categorized according to their working (image or frequency) domain, they can also be categorized according to the data they use for coil sensitivity information. Scientists have different approaches on this calculation. Some make the use of prescan signal data which is handled as the initial step in MRI examinations, while some of them prefer acquisition of additional signal lines in k-space to estimate the coil sensitivities. Some others use combinations of collected additional signal informa-

tion and prescan data. In addition, in the scans where coil and/or table moves during subsequent acquisitions in order to take a set of images (slices) of the object, coil sensitivities can be extracted from all of collected signal data during the whole examination. However, the object should not move throughout the examination duration. Otherwise the sensitivity data is affected from the object movements and will be useless.

Hence, the methods for obtaining coil sensitivities can be examined in four categories:

- Coil Sensitivity in Image Domain

- Auto-calibration Methods

- Prescan Combined Approaches

- Dynamic Coil Sensitivity Extraction

All of these categories are explained and the related studies in the literature are given in the following subsections.

2.1.2.1   Coil Sensitivity in Image Domain

In accelerated scans, the missing signal lines in k-space resulted in aliased (folded over) MR images. Clinically, such images are useless and therefore need to be unfolded before they are interpreted by the radiologists. The folded images can be unfolded using spatial sensitivity information of the coils. The methods in this category work on the image domain. Therefore, their main aim is to reconstruct the images in order to unfold the aliased images. Figure 2.1a illustrates a folded over image because of missing lines in k-space data in an accelerated scan with an acceleration factor 2. Figure 2.1b is the reconstructed unfolded version of the image which is generated using the SENSE method.

In the image domain, pMRI method SENSE is the most popular one, and SMASH is the second. These two methods are currently implemented in the MR machines'

17

(a) Aliased image constructed because of missing k-space data.
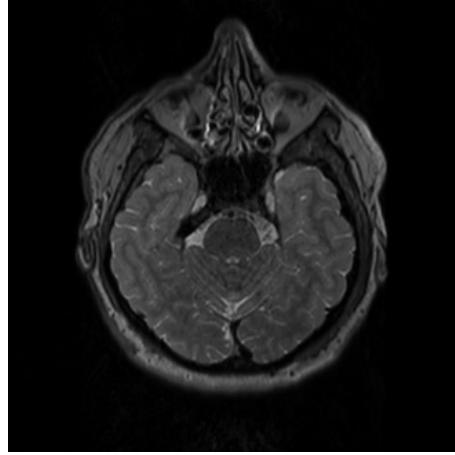
(b) Unfolded version of the image, which is reconstructed with SENSE method.

Figure 2.1: Folded and unfolded version of trans-axial head slice.

software which are commercially available in the market. Other than these two methods, there are many other important studies on image domain. However, SENSE and SMASH are like corner stones of the image domain techniques, because there are lots of studies which specifically concentrated on the improvement of either SENSE or SMASH.

The image domain pMRI method which is embedded in our scanner is explained in [58]. It is a modified version of the SENSE and is commercially available with the name of mSENSE. In our experiments, we compared our results with the outputs produced by the mSENSE technique. After introducing mSENSE for commercial scanners, the authors also made improvements on this method in study [59]. In this study, by using reference lines, the SNR performance of mSENSE was improved. Original SENSE method is also improved over time. For example, the author of SENSE technique published a novel study [74]. In addition, an enhanced version of SMASH was developed in [75].

In some of the earlier studies, the coil sensitivities were not directly used in pMRI. For example, in study [76], scientists proposed a spatial adaptive matched filter for coil array combination. Then, this method was used for reconstruction purposes in pMRI [77]. However, in almost all other image domain approaches, coil sensitivity maps were considered as one of most important data in parallel image reconstruction. Even though there are different ways of finding these maps, one of the most common

18

way requires additional data acquisition from a uniform coil (normally body coil). In this approach, the images from the surface coil are divided by the uniform coil images to find the coil sensitivities [38]. There are also other approaches on forming coil sensitivities as in studies [78] and [79]. In these methods, instead of using an additional uniform coil image, they found the surface coil sensitivities using signal processing techniques, namely, wavelet denoising and smoothing.

Up to this point, we mentioned some of the methods which use coil sensitivity maps in image domain pMRI. However, in study [80], images with sparse representations were recovered from randomly under sampled data without using the sensitivity maps. This method is based on mathematical theory of compressed sensing. This way, scientists achieved better resolutions and accelerated acquisitions.

2.1.2.2 Auto-calibration Methods

Auto-calibration methods acquire the sensitivity information during (immediately before or after) the actual scans via collecting additional signal data. Thus, problems caused by the motion of the patient after each scan session is diminished. However, moves during the scan acquisition is still a problem. This technique is particularly useful when the coil or the patient moves after each subsequent scan. For example, in moving table acquisitions (i.e. imaging slice position is adjusted by table movements), significant changes can occur among the sensitivities of each slice during the whole examination session. In such cases, auto-calibration methods provide much better results as the sensitivity data is calculated for each slice separately.

Auto-calibration methods require acquisition of extra signal data in each scan for sensitivity calculation and this increases each individual scan time. Therefore, the main motivation among the studies in this category is keeping this additional signal data as small as possible. In these methods, a low resolution central full k-space data is acquired as well as the interleaved high resolution actual accelerated scan data. The former data is used for calibration and sensitivity map extraction and the letter is used for production of the image data. Some of the well-known auto-calibration studies in the literature are: AUTO-SMASH [64], VD-AUTO-SMASH [65], GRAPPA [39], mSENSE [58], and the study in [81].

Currently GRAPPA and mSENSE are the two methods that are implemented in commercial MRI machines. They both uses auto-calibration lines, however, while GRAPPA is a frequency domain technique, mSENSE is an image domain technique.

2.1.2.3 Prescan Combined Approaches

In prescan based approaches, the coil sensitivities are found by using both the body coil and the surface coil signal data [38]. In this approach, in order to find sensitivity map of a slice, surface coil image of a slice is divided by the body coil image of the same slice (which is assumed to be uniform). Details of this process are explained in [35]. Moreover, since a uniform image is available, prescan data can also be used for solving coil in-homogeneity problem in the images. This process is explained in [82]. In lower magnetic fields (up to 1.5 Tesla) body coil images are almost uniform therefore the sensitivities can be found correctly. However, as the strength of magnetic field increases (equal or greater than 3 Tesla) uniformity assumption of body coil images fail. Since the noise is inevitable in both coil images, division process causes additional errors resulting in artifacts.

Unlike the lungs and the heart, the head is not a regularly moving organ, and if possible, patient can be asked not to move his/her head during the entire examination process. If this can be done by the patient, prescan will be an option to estimate the coil sensitivities at the beginning of the examination and can be used afterwards (in the entire scan process). However, there is always a risk that patient can change his/her head position and this requires additional prescan. In case of the movement the computed sensitivity maps will be invalid and they should be recalculated with additional prescan session. Moreover, the movements should be tracked and the prescan data should be renewed after each movement.

In [83], the advantages and disadvantages of auto calibration methods have been discussed. The authors mentioned that the coil elements are becoming smaller with phased arrays. In the examinations where small coils are used, any coil position change during examination process affects the sensitivities significantly and movements of the scanned subject during the entire MRI examination cause crucial problems.

1	1
2	2
3	3
4	4
5	5
6	6
7	7
8	8
9	9
10	10

(a) First image frame of adjacent slices   (b) Second image frame of adjacent slices

Figure 2.2: a) Adjacent k-space data for first and second MR slices in dynamic acquisition. Missing lines are shown as dashed lines. Using adjacent slice information, coil sensitivity can be found by merging the two k-space data.

2.1.2.4 Dynamic Coil Sensitivity Extraction

Compared to the previous coil sensitivity calculation techniques, dynamic coil sensitivity calibration approach is relatively new. This method can be used if more than one MR slice is going to be taken into account and the coil (either itself or with the patient table) is moving during image acquisitions. This way, the missing lines are scanned in the adjacent slice acquisition, therefore, these lines can be found by merging the information in the adjacent frame signal values. The acquired and missing lines in each slice are shown in Figure 2.2. The missing even numbered lines are replaced in the next slice. Thus, without the need of extra calibration lines, the required coil sensitivities can be found by combining the two adjacent slice information.

The well-known methods using dynamic coil sensitivity technique are TSENSE [84] and TGRAPPA [69]. As in SENSE and GRAPPA methods TSENSE is applied in the image domain and TGRAPPA is used in the frequency domain.

The techniques in this category have some limitations. For example, the slice positions should be selected properly and all of them should be located in parallel. Moreover, since the techniques require coil movement in a particular direction, during the movement, the subject should not change its position. Any change will result in artifacts in the reconstructed images. Furthermore, the movement in any direction cannot be possible, therefore, slice positions and orientations are limited in these techniques.

2.1.2.5 Discussion on Sensitivity Extraction Techniques

If the coil shape or position is fixed and the patient is not moving, prescan gives better results in coil sensitivity extraction and, therefore, the parallel reconstruction. Since this calibration step is done once at the beginning of the examination and is used in all other actual scans, the time increase in an overall scan is very limited. In addition, it is possible to create high resolution sensitivity maps by increasing the prescan resolution. However, this means additional time requirement for the prescan process. In case of a change in the imaging subject or the coil position, the prescan process should be repeated, otherwise, this causes significant changes in the sensitivities resulting in images with artifacts.

An alternative option is getting some extra reference lines in each scan to estimate the coil sensitivities but this increases the scan time considerably. This contradicts with the main aim (increasing the speed of acquisition) of pMRI. Moreover, increase in scan time may cause additional problems. For example, for the claustrophobic patients, the MRI examinations will be even harder. Moreover, in some cases, increase in the time means exposure of the side effects of MRI (such as RF and its side effect heat) for a longer duration, which is harmful to human body. Furthermore, as stated in [85] and [86], since the reference lines provide low resolution images, they are susceptible to Gibbs phenomena [87].

If the slices are going to be in the same orientation and the coil can be moved accordingly, then dynamic coil sensitivity methods will be better but they have also limitations such as the subject should not move within the examination.

In short, depending on the examination conditions, the better method in terms of coil sensitivity mapping may change and therefore the success of the parallel MRI reconstruction. A recent study [37] reviewed the pMRI methods in different aspects.

2.1.3 The Proposed Parallel Imaging Approach

In this dissertation, we focused on a commercial head coil shown in Figure 2.3 (Siemens 32 channel Head Coil [1]) which is fixed to the patient table and is rigid

22

in shape (i.e. it shape does not change in any condition and is not flexible). Since it is stuck to the table, finding the coil position and then the image slice positions from the table location information relative to the coil is a trivial problem. A novel method is proposed for coil sensitivity computation to achieve the following aims:

- The provided method should minimally be affected by the patient movement

- The generated sensitivity maps should have at least the actual image resolution

- The method should not increase the MRI examination time

Although we worked on a head coil, the study can be extended to the other surface coils. In addition, head imaging has a great importance in MRI. Head scans constitute a significant percentage (22% in the United States [88]) of the MRI examinations, and most of the available head coils are rigid and attached to the table. Moreover, for claustrophobic patients, the most challenging scans are again the head scans. According to [89] and [90], head and nerve system MRI provide a more comprehensive information than any other medical imaging technique and it is the most sensitive scanning test of the head in clinical practices. Thus, any improvement on the quality of head MR images and scans will have significant impact towards clique practices, which is the main motivation behind this study.

Thus, all the methods for coil sensitivity estimation in the literature have several benefits with unintended side effects. To solve this problem, we propose a novel method to build coil sensitivity maps. Instead of estimating the coil sensitivities using additional accusations before, after, or during the actual scans, we directly calculate them using the coil internal wire shape information. This new method is based on coil wire position information and Biot-Savart Law (equation [1]). When the sensitivities are found, unfolding the overlapped images caused by reduced k-space lines and fixing surface coil image in-homogeneities become possible with the known pMRI methods. Currently, this method can be used only when the coil position is known and fixed in each scan during an examination like the head coils which are fixed to the table.

Figure 2.3: Siemens 32 Channel Head Coil.

2.2 Intensity In-homogeneity Correction in MRI

Even though MRI is one of the most important medical imaging devices, it is not perfect in terms of the quality of the images that it produces. There are several artifacts which degrade the quality of the images. According to the [91] some of the common artifacts in MRI images are as following.

- RF Offset and Quadrature Ghost

- RF Noise

- B_0 Inhomogeneity

- Gradient

- Susceptibility

24

- RF Intensity Inhomogeneity

- Motion

- Flow

- Chemical Shift

- Partial Volume

- Wrap Around

- Gibbs Ringing

- Magic Angle

There are several reasons behind these artifacts, but, as we used a head coil, we concentrated on **RF Intensity Inhomogeneity artifact** which is directly related with this hardware. It is caused from either non-uniform B_1 field or, by nature, non-uniform sensitivity profile of receive RF coils as in our coil ([1]).

While RF in-homogeneity artifact does not cause a significant problem in lower fields ($B_0 < 3$ Tesla), in higher fields, this problem becomes apparent. Presence of the artifact can affect the decisions of the radiologist on diagnosis and staging of several diseases like cancer. In addition, artifacts reduce the quality of automated post processing techniques such as image segmentation and registration which gives quantitative measurements on the images.

In the literature, there are several studies trying to solve this problem. Some of them are post processing techniques, while some others are in-processing methods which are applied during MRI acquisitions. A common way to fix the in-homogeneity problem is to find intensity correction maps, then applying these maps on the real images to generate more uniform images. There are several ways to find these maps.

The first method is obtaining the maps from in vivo images. [92] is an important study which illustrates this technique. It proposes a special excitation pulse to compensate for RF in-homogeneities especially for brain images. According to the results of this study, images acquired with this excitation pulse, without using intensity correction algorithms, images can be segmented. Another study is [93], which uses two images

with different flip angles (θ and 2θ) to fix the in-homogeneity problems. From these two, first spatial distribution maps are created and then new images are corrected by division process with the found spatial distribution maps.

The second method takes additional images on uniform phantoms from the scanner to find the intensity changes over the imaging medium. There are several studies using this approach to fix the image non-uniformities. For example, in the study [94], a uniform phantom is used and the actual images are normalized by division of phantom images.

The third method is estimating the correction maps by using statistical information extracted from the images. A sample study in this category is [95] where, a simple statistical based rapid correction algorithm is proposed. In this method, first, the noise of the image is calculated and then, the average signal intensity of the non-noise locations are determined and after these operations, the noisy part of the image is filled with average intensities of non-noisy parts. When all these operations are applied to the image, the final steps are smoothing and normalization of the image.

The fourth method is to create theoretical modeling approaches to find the maps. One of the recent and important studies in this category is [96]. In this study, an iterative and fast approach is proposed for in-homogeneity problem.

Each of these methods has its own advantages and disadvantages over the others. A detailed review was given in [97]. There are also several other important studies on in-homogeneity problem such as [98], [99], [100]. [100] reviewed almost 60 studies and categorized them. According to this study and [98], the in-homogeneity issue is not a completely solved problem and therefore in the future, will continue to receive attention from scientists. [99] compares six of the well-known intensity non-uniformity correction algorithms in different conditions especially in lower and higher fields. According to this study, none of the methods performed ideally under all circumstances but locally adaptive methods are better than the general ones.

To sum up, image non-uniformity is still a current problem in MRI images. Even though there are several studies providing solutions to the problem, with the advances in MRI technology (like higher magnetic fields and multi channel coils becoming

available) the problem arises while the old approaches fail. For example, in higher fields, uniformity assumption of B_0 field fails therefore correction methods using division process fail as a result. Moreover, in multi-channel surface coils, the sensitivity change of the RF receivers over the image is not always smooth. The reason for this is that the image is constructed with the help of several coil elements. Since the sensitivity changes of receive RF coils over the imaging slice is complicated, this makes the in-homogeneity issue even more complicated.

According to [98], to solve the in-homogeneity problem the first focus should be on the real causes of the issue. Therefore, in our study, we focused on the sensitivity changes in the receive RF profiles of a surface coil [1]. Our assumption depends on the fact that if the sensitivity profile of a coil is computed precisely, then non-uniformity caused from the sensitivity changes will be fixed trivially. Therefore, in this study, complex sensitivity profiles of the surface coil is calculated and the in-homogeneity problem caused from the sensitivity changes is fixed accordingly. The details of our approach will be explained in the following chapters.

CHAPTER 3

THEORETICAL BACKGROUND

In MRI world, radio frequency (RF) coils act as antennas of the system. Coils send RF signals to the body of patient and receive the return signals from the body. Some of them work as RF transmitter, some of them as RF receiver, and some others work as both transmitter and receiver. Most of the time, body coils work as transmitter and provide nearly uniform RF field (providing that the main magnetic field strength is less than or equal to 1.5 Tesla) using more energy when compared to the surface coils. On the other hand, surface coils have better signal receive characteristics as they are located close to the subject. Therefore, when receiving the RF signals from the body, surface coils provide better information in terms of signal to noise ratio (SNR). However, their receive ranges are very limited and their sensitivities to the signal significantly changes going farther away from the wires. The coil sensitivity decrease is nearly inverse proportional to the square of the distance from the coil wires. Therefore, the sensitivity change depends on the shape of the wires inside the coil and their relative distance to the imaging subject.

MRI magnetic fields inside the MR machine are represented with two abbreviations/symbols. They are B_0 and are B_1 and are explained as follows:

- B_0 : The symbol used for the main magnetic field strength in the MRI system. This value is constant and nearly homogeneous in the MR machine. The direction of the main magnetic field defines the longitudinal axis of the system and is also represented with B_0 symbol.

- B_1 : The symbol used for the RF field strength in the MRI system which is

perpendicular to B_0 [101]. This field is mainly produced by the surface RF coils or the tissues of the patients and is used for adjusting the magnetic field strength inside the MR machine. It has two circularly polarized components as: B_1^- (receive RF field produced by the body tissues) and B_1^+ (transmit RF field produced by the surface RF Coils) [102]. In this study, we are interested in RF receive field (B_1^-).

3.1   RF Receive Field B_1^-

Coil sensitivities can be calculated using the reciprocity principle. It was shown that the spatial distribution of the circularly polarized component of the magnetic field, B_1^-, generated by the coil element when a unit current is applied to the terminal of the coil, is proportional to the sensitivity distribution of this coil element. In this study, we assume that the size of the coil is small (has a diameter less than 10 cm) and it has a simple loop structure (not necessarily circular), and the current applied to the terminal of the coil remains unchanged on the wire of the coil.

According to [103], the reciprocal fields can be calculated using Biot-Savart integration when the object size is smaller than the RF wavelength. If this condition is preserved, the geometry of the RF field is hardly affected from the presence of the scanned object. In this study, our target object is the human head and the typical human head sizes are listed in [104]. In addition, typical human head sizes in the United States are listed in [105]. As it is stated in [106], RF wavelength on average for *in vivo* brain imaging is 27 cm at 3 Tesla and this is greater than the typical human head sizes. In addition, sensitivity area of a coil depends on its diameter and the sensitivity of the coil is decreased rapidly with increasing distance away from the surface [107]. The region where each coil channel retrieves a high signal is even shorter than the head size as shown in Fig. 3.1c. Therefore, in phased array coils, each channel is arranged properly to get the maximum image quality.
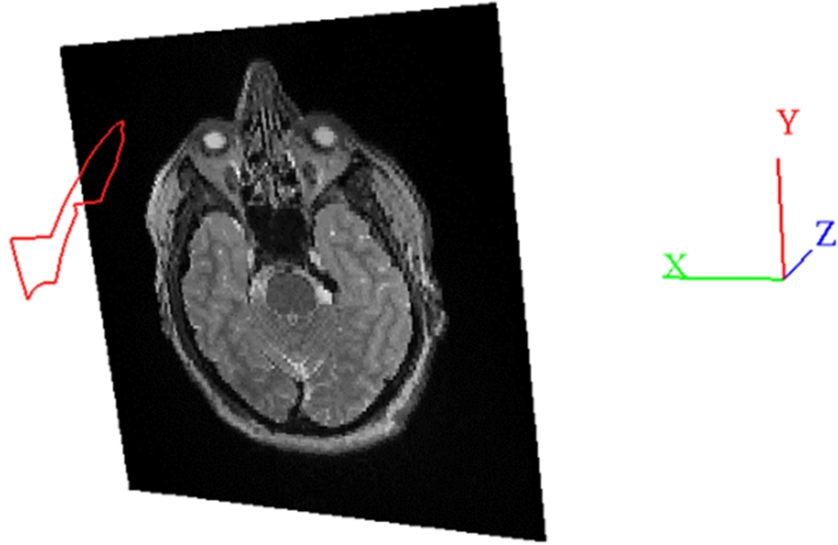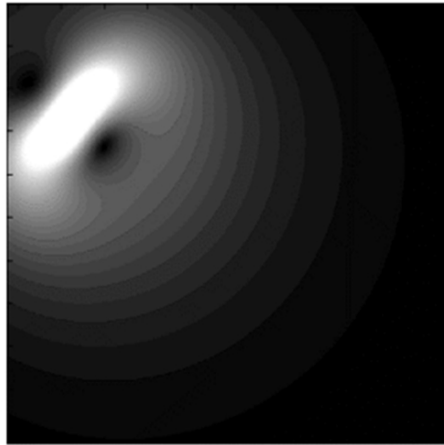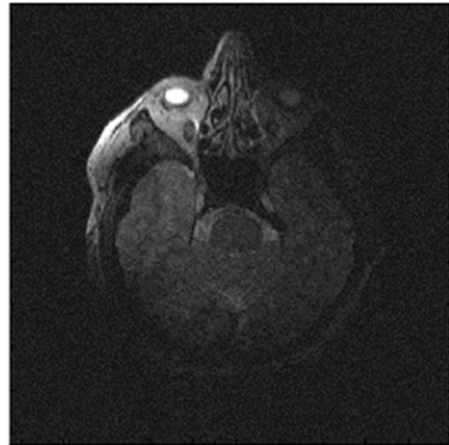
Figure 3.1: Sensitivity map calculated from an element of the 32 channel head coil. (a) 3D model of a channel and slice position; (b) Sensitivity map; (c) An image obtained using only this element of the coil.

3.1.1 Biot-Savart law

Electric current carried by a wire creates magnetic field. The strength of this field at a point of interest in the space can be calculated using Biot-Savart law (Eq. (3.1)). This law can be used in MRI under quasi-static assumption, as the magnetic field contribution of a unit current on an infinitesimal wire segment, $\overrightarrow{dl}$, at position $\overrightarrow{r}$ with respect to the point of interest [108]. According to [109], this assumption is valid if the receiver coils are much smaller than the wavelength at the Larmor frequency. The RF field wavelength outside the body is 234 cm and approximately 30 cm inside the body at 3 Tesla [110]. All this information makes our assumptions valid for such a study since our head coil element diameters are about 8 cm for all channels. Then, we can calculate the magnetic field as:

$$\overrightarrow{dB} = \frac{\mu_0}{4\pi |\overrightarrow{r}|^3} \overrightarrow{dl} \times \overrightarrow{r} \tag{3.1}$$

where μ_0 is the constant representing the permeability of free space and we assume body has the same free-space permeability.

According to Biot-Savart Law, magnetic field strength of a position near the wire depends on the magnitude of the current and the distance from the wire. In MRI, a similar but opposite event occurs. Instead of a giving current in to the wires of a surface coil to produce magnetic field, electro-magnetic signal goes over the wires of the coil. This produces an alternative current in the wires in small amounts. The induced current in the coil is first amplified from the MRI machine, then is transformed into signal data and finally converted into the images after some image and signal processing operations by the computers of the MRI machine.

3.2 Physics Behind MRI

A typical MRI examination has following steps:

- Body is located inside the main magnetic field of the MR machine.

32

- RF at Larmor frequency is transmitted into the body part which is going to be imaged by the transmit coils for a period of time.

- Electro-magnetic signals are released from the atoms of the body after the RF pulse is turned off from the transmit coils.

- Emitted signals by the body internals are collected from the receive coils and amplified from the MRI machine.

- Collected RF signals are saved into the machine and then processed. These signals are converted into MR (DICOM formatted) images.

It this study, it is assumed that the strength of magnetic field at a position next to a coil due to a unit current in its wires is directly proportional to the sensitivity of the wires at the position when there is an electromagnetic signal which is broad-casted from the atoms of the body part at that position.

Actually, this assumption is not valid in all cases. There are several factors that affect the electromagnetic signals originated from the atoms until they reach to the coil. Not only the distance between the point of interest and the coil wire but also some other factors, like changes in electric properties (i.e. conductivity and permittivity) of the tissues, can affect the electromagnetic field signals reaching to the coil wires. In this study, we ignored the factors other than the distance. Provided that the size of the phased array coil is small and the region that the coil gathers signal (i.e. the region visualized from the coil) is narrow, any other effect does not create significant deviations at the signal level. However, for larger coils, this assumption may not be correct. Such effects are going to be analyzed over electromagnetic simulations in the next chapters. Holding our assumption, the sensitivities of coils can be calculated using the reciprocity principle if its exact wire shapes are obtained using Biot–Savart law.

In pMRI, when the sensitivity maps are used for unfolding the overlapped regions, the exact result (i.e. the exact magnetic field values) of equation in 3.1 is not required. However, the ratio of sensitivity change over the imaging slice is necessary. Therefore, any fixed value can be used for the constant μ_0 since it is only a multiplier in the equation. In addition, it is assumed that any other effects on the sensitivities such as

the body load, tissue dielectric property variations or the coupling effect between the coil elements are ignored. Therefore, we assumed that the multiplier is constant over the imaging region.

CHAPTER 4

THE METHOD

The main aim of this study is to find more accurate spatial coil sensitivity maps than the ones in the existing methods, by using MR scan data and geometry of the array elements, then, using the maps to construct better images. The proposed method has two steps:

1. Sensitivity map derivation

2. Parallel image reconstruction

4.1 Sensitivity Map Derivation

As we stated in the previous chapter, this study is based on the following assumptions:

- Sensitivity magnitude of coil element at a position in the space is directly proportional to the magnetic field strength at that location when there is a unit current in its wire loop. The prerequisite of this assumption is that the imaged object size should be smaller than the RF wavelength at the Larmor frequency. If this condition is satisfied, according to [103], the magnitude of the magnetic field variations due to load (body) can be ignored for coil elements with a diameter smaller than RF wavelength.

- There is no coupling effect between elements of the coil, or the existing coupling effect is so small that it is negligible.

- The coil tuning is nearly optimal therefore there is no significant factor which alters the coil sensitivity profiles.

Coil sensitivity maps are complex-valued data that can be represented in terms of magnitude and phase information. In this study, these two distinct values are found separately and then are combined to form the complex-valued final maps. Eq. 4.1 shows the formula of a typical sensitivity map (S) derivation using magnitude (M) and phase (P) information.

$$S = M \times e^{jP} \tag{4.1}$$

4.1.1 Magnitude Data

The 3D sensitivity maps of each channel in a multi-channel coil can be computed using Biot-Savart law (eq. 3.1). The shape of wires in each channel can be defined as a combination of several finite straight wires while calculating the magnetic field (B) using Eq. 4.2. In the equation, μ_0 represent permeability of the free space which is approximately the same as the human body. Other parameters are explained in the next paragraph on a figure. If the coil shapes cannot be defined with a combination of discrete wire segments (such as circular or elliptical shapes), the sensitivities can be calculated with proper methods in the literature which are used for magnetic field calculation purposes. Since the coil channels used in the study can be defined as a combination of finite wire segments, only this sensitivity calculation process is explained.

$$B = \frac{\mu_0 I}{4\pi R}[cos(\alpha) + cos(\beta)] \tag{4.2}$$

Fig. 4.1 presents an illustration of magnetic field at a position, P, due to a current I in a straight finite wire. Distance, R, and angles α and β can be seen in the figure. The x and y components (z is the B_0 (main magnetic field produced by the MRI machine) direction) of the magnetic field for each current segment can be calculated using geometrical position of the wire segment and using the right hand rule. Using
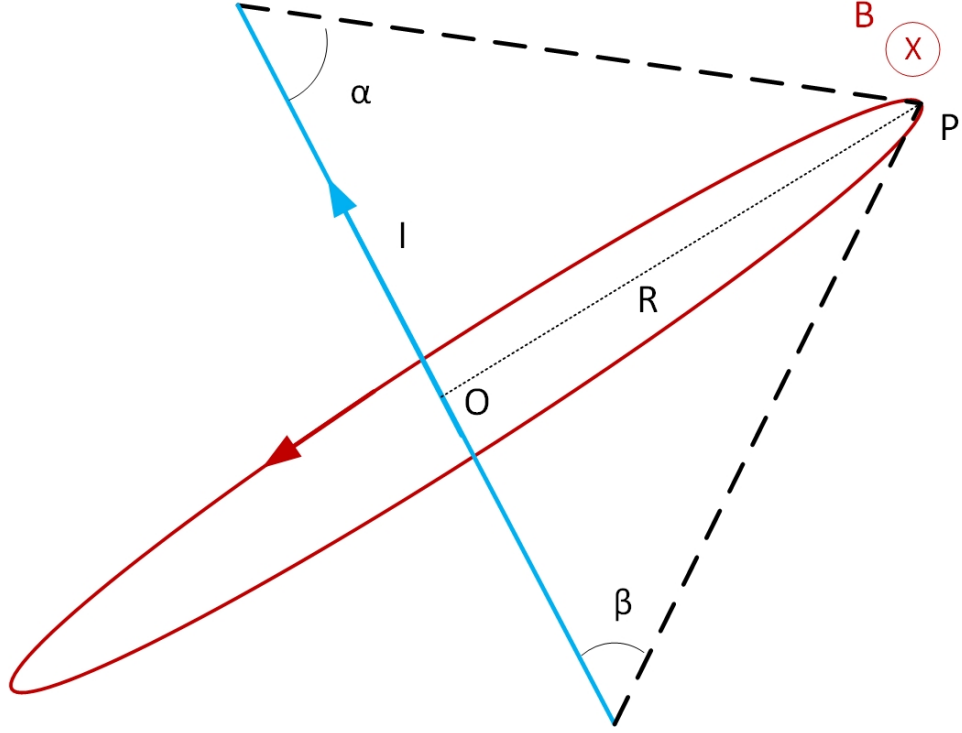
Figure 4.1: Magnetic field generated at point P by the current I in a finite straight wire (shown in blue). Magnetic field on the red circle is constant and tangential to it. The angles α and β are used in equation (4.2) in order to calculate the magnitude of the magnetic field.

this information, the complex value, B_1^-, can be calculated as the sensitivity of the coil by applying summation operation on all current segments. Afterwards, the complex numbers are converted to the absolute values by applying *abs* function in MATLAB to find the magnitude information.

Using these processes, for each voxel inside the imaging plane, a sensitivity value is calculated for each element of the head coil. For illustration, a sample coil element is shown in Fig. 4.2 as an octagonal wire. In the same figure, the patient head is shown as a sphere. The B value is the summation of magnetic fields produced by all wire segments $W_1, W_2, ...W_n$. That is $B = B_{w1} + B_{w2} + ...B_{wn}$. The magnitude of B vector is calculated by $abs(B)$ in MATLAB.

For experiments, a 3T [111] MRI scanner was used. In order to demonstrate the performance of the new method, we obtained images in normal (without acceleration) and in SENSE (commercial name is mSENSE [58] in our scanner) modes. Moreover,

the 32 channel head coil [1] was used in the experiments and it has the outer dimensions of 300 mm × 309 mm × 290 mm (L×W×H). The coil inside where the human head is located is sphere shaped and the internal diameter size is about 22 cm. Each of the coil elements has a diameter of less than 10 cm. According to head sizes given in [104], it is expected to have a minimum of 1-4 cm distance between head and each coil element.

Scan data contains table location and corresponding slice position information. All these values are given in machine's coordinate system. Therefore, image position with respect to head coil location was found and the position of the coil wire loops were calculated for each image. We obtained the sensitivity values for a volume of coil size (where head is located) with a resolution of 1mm x 1mm x 1mm voxel size (a better resolution can also be calculated). Thus, the spatial coil sensitivity magnitude data of the head for each channel is obtained. Moreover, we prepared a 3D model of the head coil and rendered it in OpenGL in order to visualize the coil elements, scan data, and the calculated maps. Fig. 3.1a presents a snapshot of the program. From the figure and the figures presented in the study [112] it is clear that a coil channel
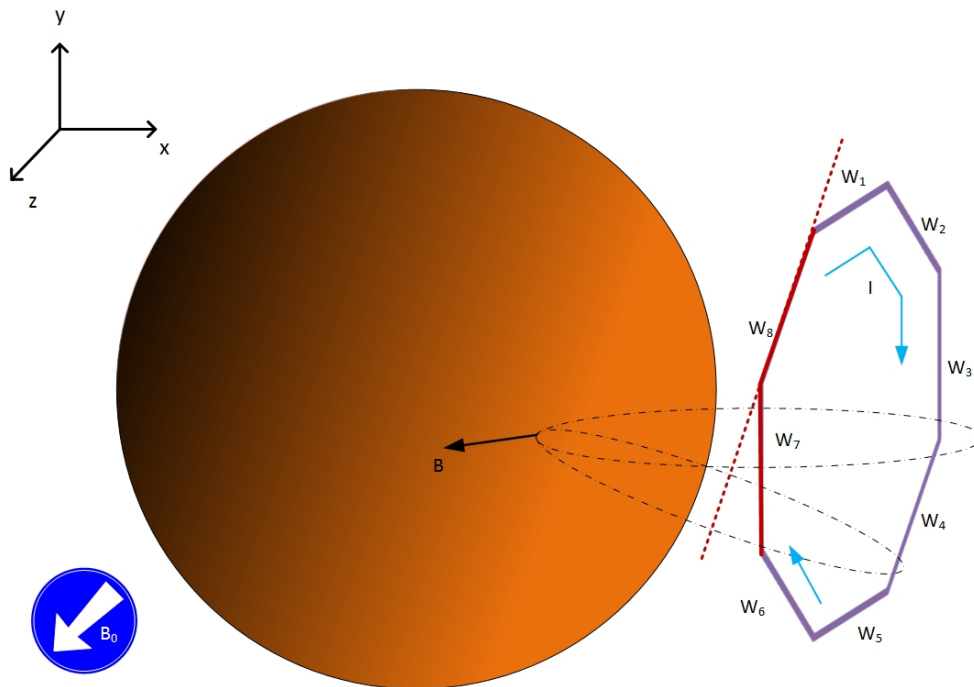
Figure 4.2: Magnetic field at a position P due to a current I in a wire loop is the vector sum of magnetic field due to each wire segment ($W_1, W_2, ...W_n$).

has complex shape. However, the method can also be applied to simple shapes like circular, square or rectangular shapes.

4.1.2 Phase Data

In the proposed method, phase information of the sensitivity maps are retrieved from the raw scan data. Instead of using the calculated B vector directions in the magnitude computations, we prefer to use the phase data in the scan signals. They are obtained from the scanner and they contain MR signal data with scan configuration information.

In mSENSE mode, our MRI machine creates two different complex type data for each channel. One is the fully sampled central region of k-space data and the other is the under sampled k-space data. MRI machine uses former data for sensitivity estimations and the latter data to form aliased images. Using the sensitivities, the machine unfolds the overlapped images and forms the full FOV images. In this study, we used the former data to construct phase data of our sensitivity maps by first applying the Fourier transform and then taking $tan^{-1}(Imag/Real)$ of the complex data. Since the scan phase information is used all of the parameters (such as body load) that may affect the phase data is take into the account. We also applied Fourier transform to under sampled data and obtained the aliased images which are unfolded after pMRI operations.

Using the phase information from the scan data is important. By using it this way, the possible difference between the actual sensitivity maps and the calculated ones with the proposed method will be smaller. Even though there is a gap between the calculated magnitude values using Biot-Savart law and the actual ones because of body load or any other reason, there will be no difference between the phase information that is collected from the low resolution data and the actual scan data.

4.2 Parallel Image Reconstruction

In order to show the success of the calculated sensitivity maps, the SENSE [38] technique is used for the parallel image reconstruction. Even though the machine uses another method (mSENSE) and it is significantly different than ours in terms of sensitivity map derivation, both are similar the way they use of sensitivities to form final images. Final images are constructed by solving a set of linear equations with an unknown number which is equal to the acceleration factor in both methods.

The acceleration factor defines the gap between each adjacent line in k-space. For an acceleration factor α in a 2D image, after acquisition of one k-space line, the next $\alpha - 1$ lines are skipped in phase encoding direction in full k-space. Thus, as the gap between the actual lines increases, the total lines in the k-space and the total scan time decreases proportional to the acceleration factor. However, since it is needed to take some reference lines for the estimation of the coil sensitivities, the net speed gain in terms of time is not equally proportional to the acceleration factor.

After the sensitivities of the coil channels are determined using the proposed method, and aliased images are formed from k-space data from Fourier transformation, the last step is to construct the final image using the SENSE method. The main purpose of the simple SENSE technique is to unfold the aliased images using the sensitivities of the coil channels as explained in [113].

The details of the parallel image reconstruction can be explained in the following two steps:

- Construction of aliased images from k-space data.

- Applying pMRI Reconstruction Method

4.2.1 Construction of aliased images from k-space data

After calculating the sensitivities of the coil, the next step is acquiring the k-space data for each scan. In this study, a 3T (MAGNETOM Trio a Tim System, Siemens Healthcare, Erlangen, Germany) MRI scanner was used. In this machine, two inte-

grated Parallel Acquisition Techniques (iPAT), which is the term used by the vendor of the pMRI method, are available. One is mSENSE [58] and the other is GRAPPA [39]. We used both of these pMRI methods, and compared the results with ours after several experiments on volunteers and phantom. The comparison of the images are done by an experienced radiologist as well.

The raw files obtained from the scanner contain signal data. Along with the raw files, the machine also provides DICOM formatted images as a final output for the radiologists. Raw files contains header information as well as signal data. In iPAT mode, the signal data is the combination of two different k-space data. One type is the under-sampled one and the other is the fully sampled, low-resolution, central region of k-space data. Former type of data is the main image signal data. The latter is called as reference lines which are used for the calculation of spatial sensitivities of coil channels. In this study, we used the former data and only the phase information of the latter one.

Figure 4.3 illustrates a sample k-space data when the acceleration factor i set to 2. In the figure, dashed lines illustrate the missing lines and the other lines represent the signal lines collected during the examination process. From the under-sampled part of k-space data, the aliased images are constructed by applying Fourier transformation. From the central region, where there are no missing lines, the sensitivity maps are found by first applying Fourier transformation and then division to the SoS of all channels sensitivities.

4.2.2 Applying pMRI Reconstruction Method

When the calculated spatial sensitivity values are obtained in the image domain instead of the Fourier domain, simple SENSE technique can be used for pMRI reconstruction. In this method, final images are constructed by solving linear equations where unknown variable numbers is proportional to the acceleration factor.

The acceleration factor defines the gap between each adjacent lines in k-space. For an acceleration factor α in a 2D image, after acquisition of one k-space line, the next $\alpha - 1$ lines are skipped in phase encoding direction. This process continues until the
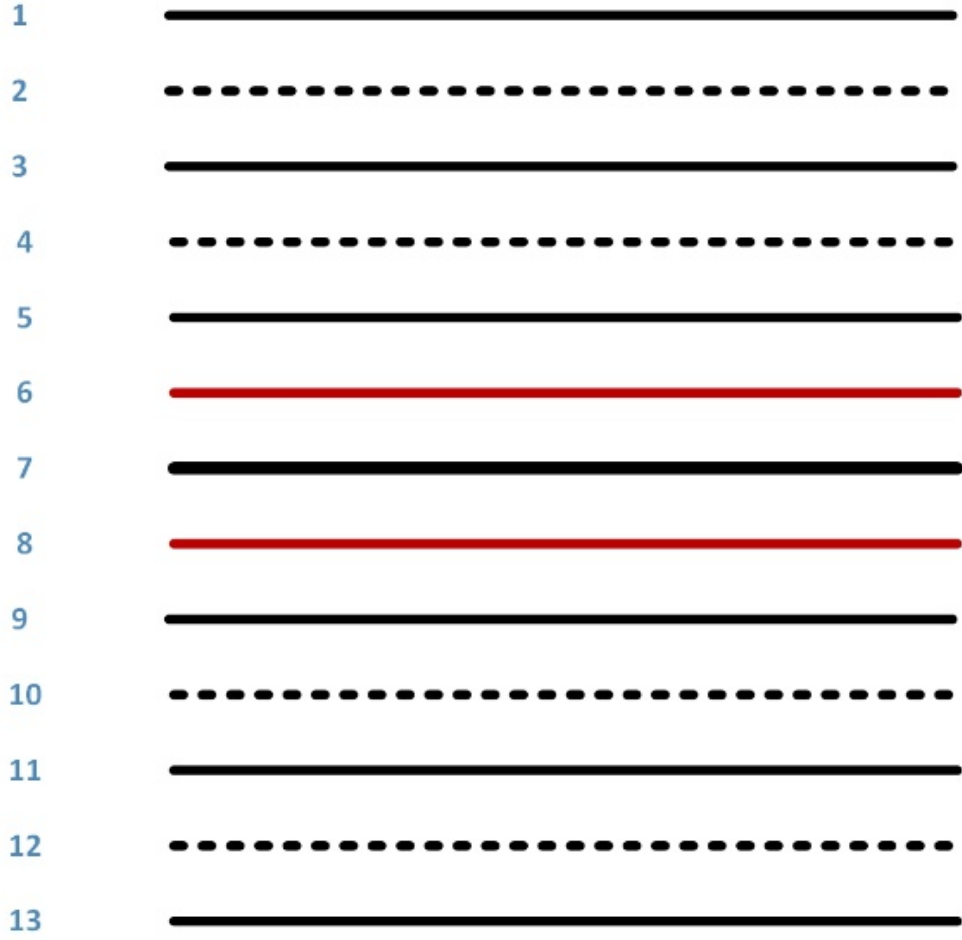
Figure 4.3: Sample k-space with an acceleration factor 2. Bold line is the center of k-space. Dashed lines (2, 4, 10 and 12) are the missing lines. Fully sampled center region (5, 6, 7, 8 and 9) is used as reference lines in calculation of coil sensitivities. Red lines are not missed to create a fully sampled region for sensitivity estimation.

formation of full k-space. Thus, in accelerated scans, since the gap between the actual lines increases with acceleration, the total lines in the k-space and the total scan time decreases proportional to the acceleration factor. However, it is needed to take some reference lines for the estimation of the coil sensitivities in a real scan, therefore, the net speed gain in terms of time is not equally proportional to the acceleration factor but a little bit smaller.

After the sensitivities of the coil channels are calculated using the spatial wire shapes with Biot-Savart Law and aliased images are formed from k-space data by applying Fourier transformation, the next and final step is to construct the final images using

SENSE reconstruction algorithm. The main purpose of the simple SENSE technique is to unfold the aliased images using the sensitivities of the coil channels. The implementation details of this technique has been explained in [113].

Equation 4.3 is the main formula used in SENSE reconstruction technique. In the equation c channels in the phased array coil, p pixels in the final desired image, and r pixels in the aliased images are used. AI refers to an $rc \times 1$ column matrix containing the aliased images of all the channels, S refers to $rc \times p$ matrix corresponding to spatial sensitivities of these coil channels and I refers to $p \times 1$ column vector corresponding to the desired unfolded image.

$$AI = S \times I \qquad (4.3)$$

In Eq. 4.3, AI and S are the known parameters. The unknown I is the final reconstructed image. It can be found by solving the linear equation. In the phase array head coil, which we used in the experiments, there are 32 channels. Therefore c value is equal to 32. The size of the aliased images varies depending on the acceleration factor α. The relation between the pixel size of the final reconstructed image and the pixel size of the aliased image is computed as follows:

$$p = \alpha \times r \qquad (4.4)$$

There are r number of unknowns and c number of equations. Provided that the rule $c >= \alpha$ is preserved, the linear equation can be solved theoretically. However, since there is always noise and some other negative factors in the MRI systems, most of the time, the acceleration ratio used in practical clinical applications is smaller than the coil channel size. In this study, we used acceleration ratio as 2 in our experiments, and we made comparison of the provided approach and the methods implemented in the MRI machine. In addition we showed the success of our method over reconstructed images and these images are also evaluated by an experienced radiologist.

CHAPTER 5

EXPERIMENTAL RESULTS

Serious of experiments were carried out to find the exact coil position relative to the patient table. The parameters that affects the orientation and location of the coil were discovered in this way. Then using this information, the computed sensitivities were figured out to be used in the experiments.

The experiments were carried out both on real data and simulated MRI scan data. The details of all these experiments are explained as below.

5.1 Experiments for Finding Coil Position

The head coil used in the experiments was attached to the patient table of the MR machine. Fig. 1.1 shows the head coil used in the experiments. This head coil is fixed on the patient table. Therefore its position relative to the table is always the same. The head coil position relative to the machine coordinate system is found by experiments. Fish oil pills were used as markers and they were attached to the coil as shown in the Fig. 5.1a. Although the position of the coil can be predicted roughly with respect to the patient table in Z (main magnetic field) direction, its exact position in each of the three axis (X, Y, Z) of main magnet coordinate system should be known precisely. The image slice positions and orientations can be retrieved from the MR machine. Using the coil position, its computed sensitivity map can be registered with each image slices using simple transformation (translation, scaling and rotation) operations.

<div align="center">(a)   (b)</div>
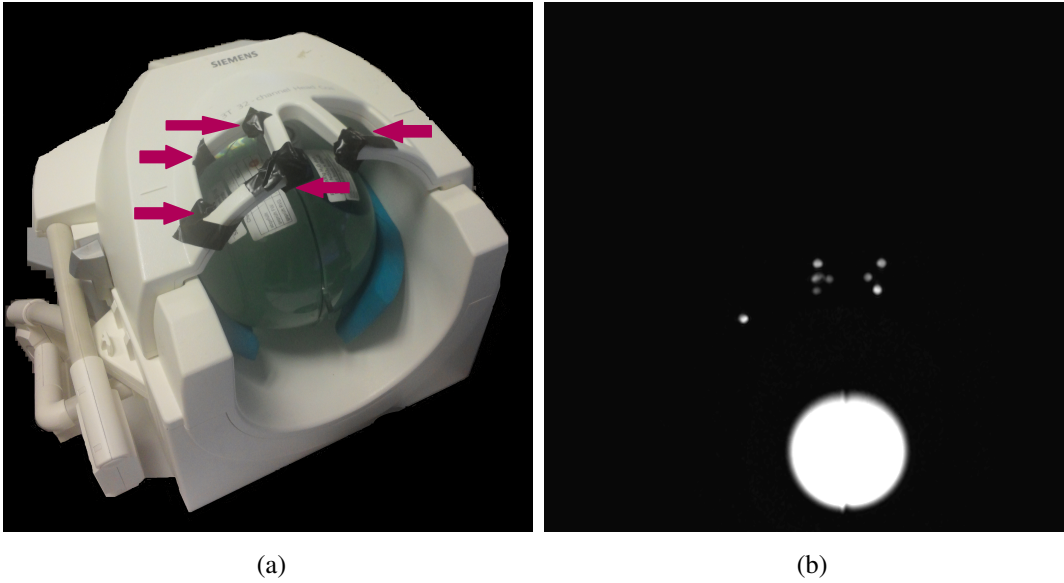
Figure 5.1: Experiment for the head coil location finding with respect to the MRI machine iso-center using oil pill markers. (a) Head coil with fish oil pills used as markers. Pill positions are shown with red arrows. (b) An image slice taken for finding the exact positions of the markers and therefore the head coil position were calculated precisely.

Markers are widely used for marking positions to be located easily in the images. One of simplest substance which produces relatively high brightness in the images is the liquid oil. In the experiments, several fish oil pills were stuck to the coil to mark the location of it in the images. Then, the distance between each marker and corners of the head coil and the patient table were measured. Since, the head coil is rigid (its internal shape does not change), once the coil position is found, the channel positions can be found easily using the 3D drawing of the head coil. Fig.5.1 is an illustration of the experiments that were made for coil positioning. In Fig.5.1a the head coil and the attached fish oil pills are shown with red arrows and Fig.5.1b is a sample slice image which is taken by the MRI machine.

After taking several image slices in different positions and orientations using the experimental setup, the head coil position was found precisely. Head coil is attached to the patient table and its position information can be retrieved from the scan data headers produced by MRI machine. Therefore, once the parameters are calibrated, the exact coil position and all of its 32 channel positions can be calculated using the 3D model of the coil for each scan. In the remaining scans, we used this calibration

parameters.

In any other coil which are not attached to the patient table the coil position should be calculated for each scan. There are several methods for finding a surface coil position during a scan and this is left as future work. They are listed as below:

- Using image processing techniques, the coil position can be found by applying matching algorithms. First intensity change over a tissue can be calculated for each channel and this change is registered by applying basic transformation operations to the found sensitivity maps. When they are registered, the coil position is also found.

- Another way is putting fixed markers on well-known positions on the coils. In each scan, using image processing techniques, first the markers are found in the image and then the coil position is calculated.

5.2 Experiments on Real Scan Data

7 volunteers and 2 different shaped phantoms were scanned and more than two thousand MR images with different scan configurations were taken in the experiments. These images were used for various purposes. The proposed method has been tested on 178 MR image slices. The experiments on human subjects were conducted with the approval of Human Subject Ethics Committee of Middle East Technical University, Turkey.

5.2.1 Sensitivity Maps

Coil sensitivities were calculated using the proposed method. The found magnitude and phase image maps are shown separately in this section.

Fig. 5.2 is an illustration of the calculated sensitivity magnitude map of an element of the Siemens 32 channel head coil. In this figure, coil element and its location corresponding to the slice position is shown in a 3D model ((a) of Fig. 5.2). Moreover,
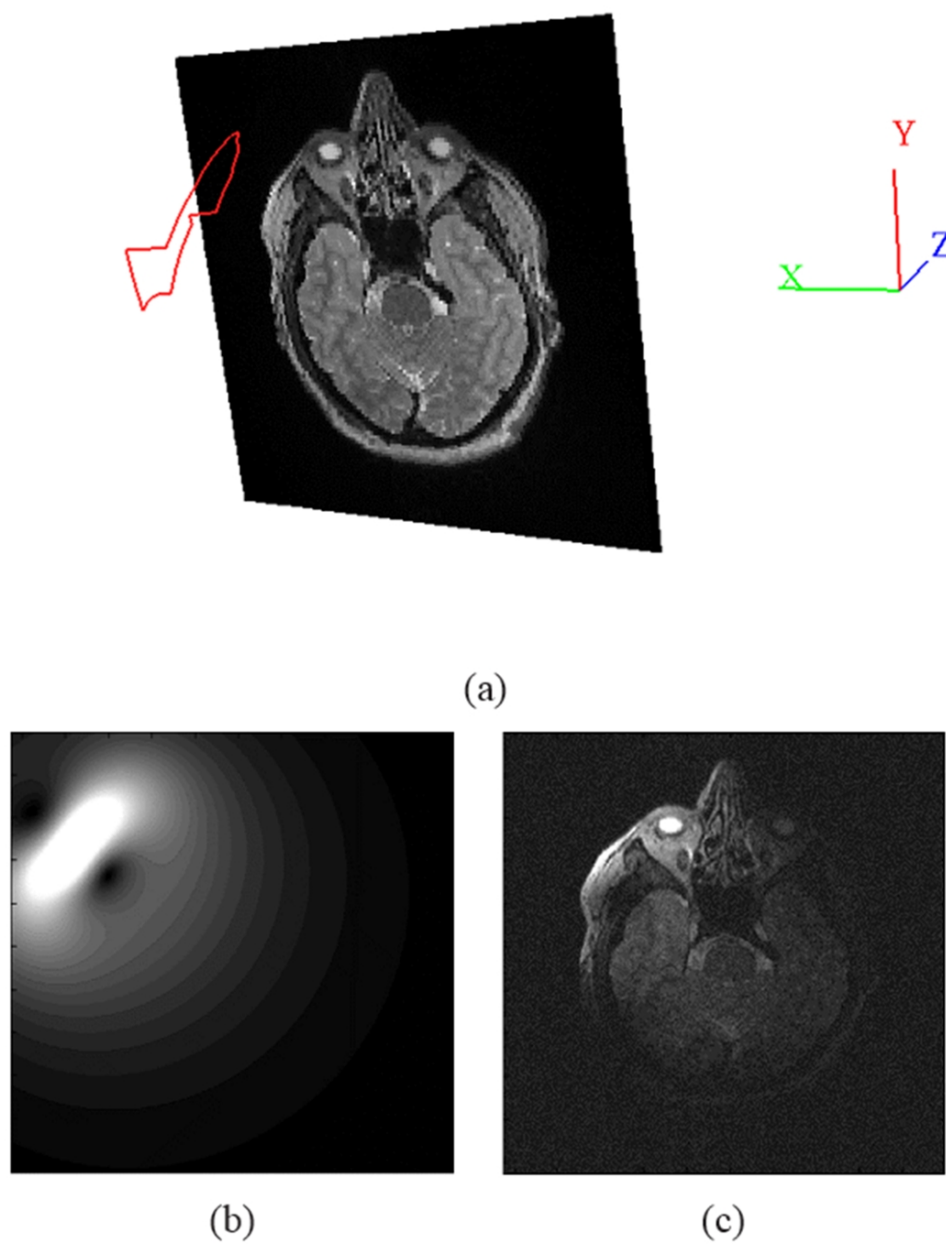
Figure 5.2: Sensitivity map calculated from an element of the 32 channel head coil. (a) 3D model of a channel and slice position; (b) Sensitivity map; (c) An image obtained using only this element of the coil.
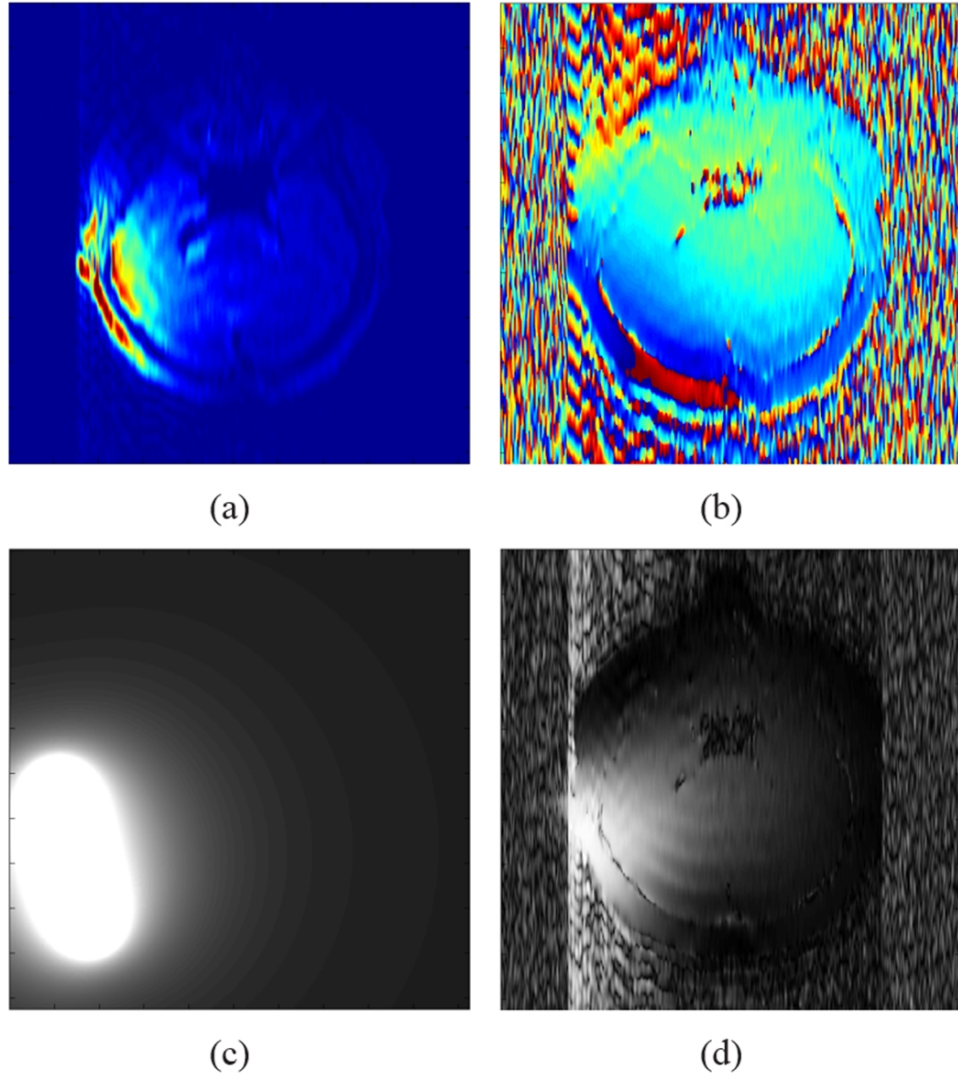
Figure 5.3: Sensitivity map calculation of a coil channel element. (a) Magnitude image of the channel constructed from reference low resolution data; (b) phase image of the channel; (c) magnitude image calculated from Biot-Savart law; (d) sensitivity map magnitude image calculated by dividing the image in (a) with SoS of all channels low resolution magnitude images.

the calculated sensitivity map ((b) of Fig. 5.2) and the channels raw image ((c) of Fig. 5.2) are also shown.

Fig. 5.3 shows the phase image generation process from a low resolution scan data corresponding to the selected coil element (shown in Fig. 5.2). The magnitude image (Fig. 5.3a) and it phase image (panel (b) of Fig. 5.3) are constructed from the scan data. When these images are compared, it can be seen that the magnitude image is affected more from the object shape and internals (such as different type of tissues)

than the phase image. Even though the signal intensities are very low in some regions, the phase information can still be extracted from a big portion of the data and therefore these images become smoother than the magnitude images. This is the main reason why we used the phase image and preferred to calculate the magnitude image using the proposed method. Moreover, for comparison, both the calculated sensitivity map and the map found by dividing the image in panel (a) of Fig. 5.3 with SoS (sum of squares) of all channels low resolution magnitude image is given in panel (c) of Fig. 5.3 and (d) of Fig. 5.3, respectively. While the calculated sensitivity map is smooth, the found map is adversely affected from the object internal structures, noise, and low resolution.

5.2.1.1   Image Samples

The images in (a) of Fig. 5.4-5.6 show SoS of absolute signal data from 32 channel. They are obtained from different slices, volunteers, scan configurations, and a phantom which are constructed by applying Fourier transformation to the under sampled raw k-space images. In each image, the acceleration factor is set equal to 2. Fig. 5.6 has different phase encoding direction than the other two (Fig. 5.4 and Fig. 5.5).

The resulting images are also provided in pairs. One is obtained by the proposed method and the other is taken from the machine. In the images, the artifacts are marked with red arrows in the magnified version of the images. The images in (b) of Fig. 5.4-5.6 show the ones obtained using manufacturers reconstruction technique, while the images shown in (c) of the same figures show the output of the proposed method, respectively. In all the experiments, the slice thickness is set to 1 mm and the acceleration factor is 2. The remaining scan parameters are provided within the figures.

The images obtained using the manufacturer's software and the proposed method can be compared in different conditions. For a detailed analysis, the magnified and color map mode versions are provided in panels (d) and (e) of the figures. Artifacts are shown with red arrows in the corresponding magnified images. The errors in the reconstructed images can be detected in the regions where no signal is expected (i.e. outside of the region where the scanned objects located). As it can be seen,
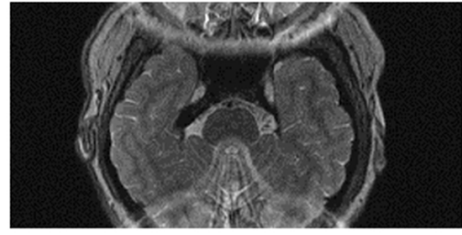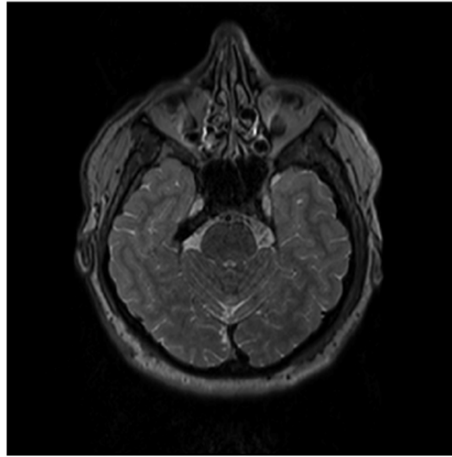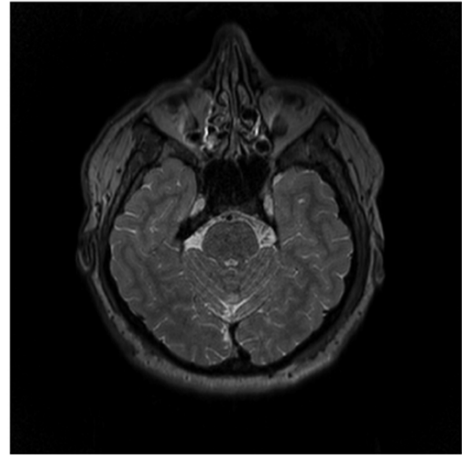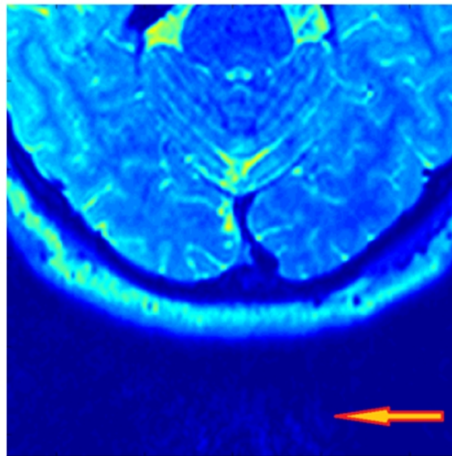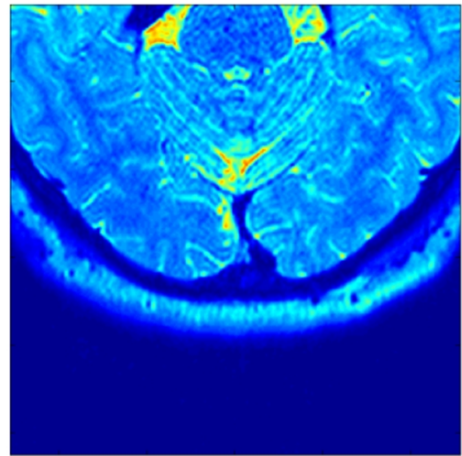
Figure 5.4: Trans-axial T2 TSE head scan experiment image data. (a) SoS of absolute signal data from 32 channel; (b) MRI scanner's output using the mSENSE method; (c) the result of the SENSE method that uses calculated sensitivity map; (d) Magnified bottom part of image given in (b) and artifacts are marked with red arrows; (e) Magnified bottom part of image given in (c).

51
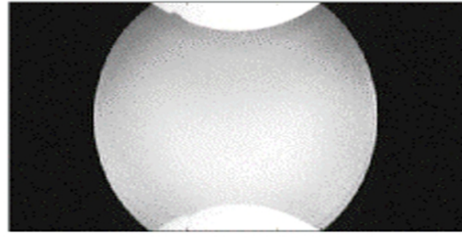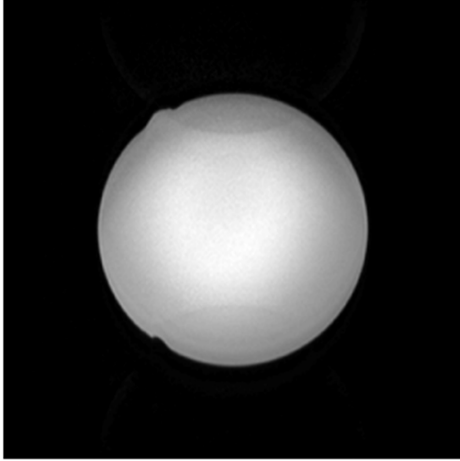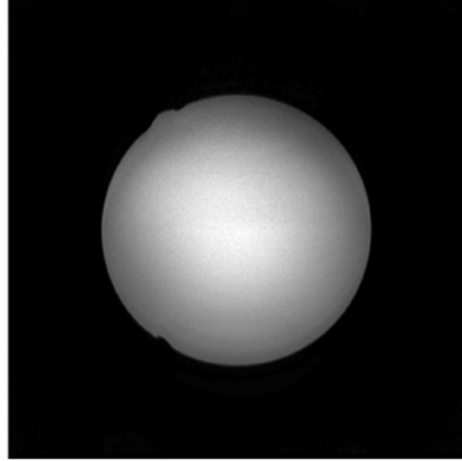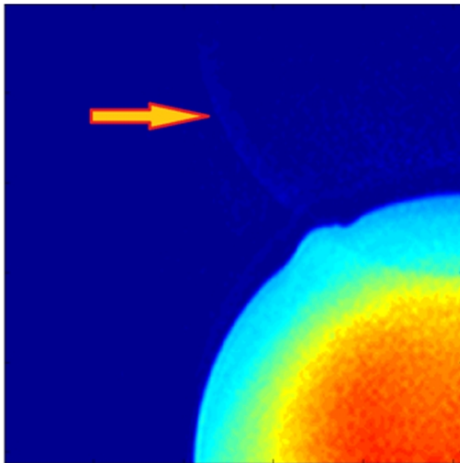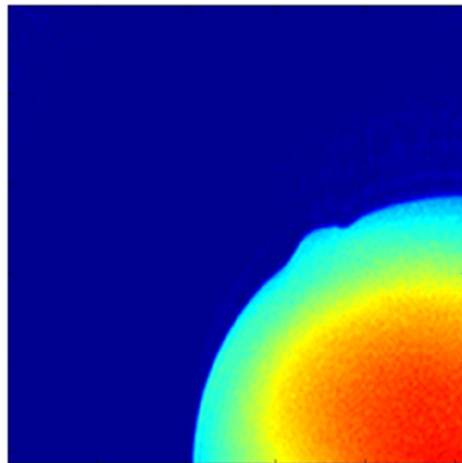
Figure 5.5: Trans-axial T2 TSE phantom scan experiment image data. (a) SoS of absolute signal data from 32 channel; (b) MRI scanner's output using the mSENSE method; (c) the result of the SENSE method that uses calculated sensitivity map; (d) Magnified bottom part of image given in (b) and artifacts are marked with red arrows; (e) Magnified bottom part of image given in (c).

the proposed reconstruction has less artifacts outside the head and phantom images indicating that the sensitivity map calculated using the proposed formulation is more accurate than the map found using acquired MR data.

In Fig. 5.7, the performance of the Biot-Savart based sensitivity calculation method on intensity correction is shown. In this reconstruction process, there is no acceleration, but the sensitivity maps are used as if the acceleration factor is equal to 1. For comparison, the machine's output image and the SoS of absolute signal data from 32 channel are also given.

5.3   Experiments on Simulation Data

A commercial electromagnetic simulation software tool (FEKO [114]) was used to simulate the B_1^- magnitude changes over a phantom depending on the coil size and distance between a coil and a phantom at 3 Tesla. Three different sized square coils were generated with a side length of 6 cm, 9 cm, and 12 cm, and a phantom with relative permittivity: 61.0 and conductivity (S/m): 0.22. These parameters were selected to simulate actual human head parameters. In the experiments, coils were positioned with a distance of 1 cm, 3 cm, 5 cm, and 7 cm to the phantom. These values were selected as the most probable distances between typical human head and the coil channels. In addition, for each experiment B_1^- magnitude values were collected with a resolution of 0.5 cm over a line starting from the coil center going through the phantom center. The magnitudes were normalized according to the point where the phantom begins. Fig. 5.8 shows a screen shot of an experimental setup and the results of each experiment.

In this study, we used the principle of reciprocity and we assumed a steady current flowing in the coil element. In order to validate this assumption, as well as the magnitude changes, we also analyzed the current variation over the coil element using FEKO simulation experiments. From the data that the tool generated, percentage of differences between the two ends of the coil conductor were calculated. These values are provided in Table 5.1, where rows represent the square coils with the provided side lengths and columns represent the distance between coil and phantom. Current

Table5.1: Current percentage change through the coil conductor

	1 cm	3 cm	5 cm	7 cm
6 cm	0.06502	0.00547	0.00563	0.00560
9 cm	0.34713	0.00091	0.00113	0.00112
12 cm	0.42000	0.00523	0.00375	0.00368

changes are less than 1% in all cases. Moreover, the current differences are maximum when the distance between the coil and the phantom is equal to 1 cm. Depending on the coil size and coil channel to phantom distance even smaller current variations were obtained. Briefly, current changes over the coil channel wires are very small and such a small change did not create a noticeable problem in the final results of the proposed method, as seen in the experiments.

Description:

Sagittal T2 TSE scan
Acceleration factor:2
FOV:200x200
Pixel Size:320x320
Phase encoding direction:
Column
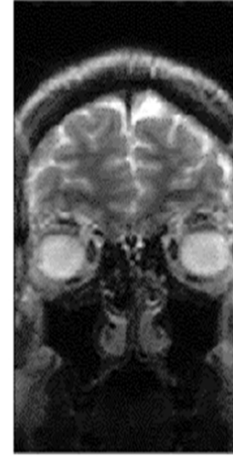
(a)
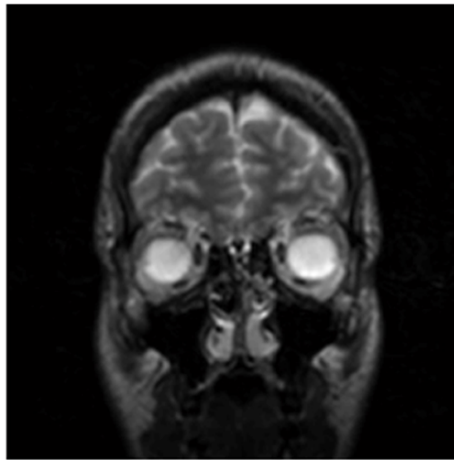
(b)
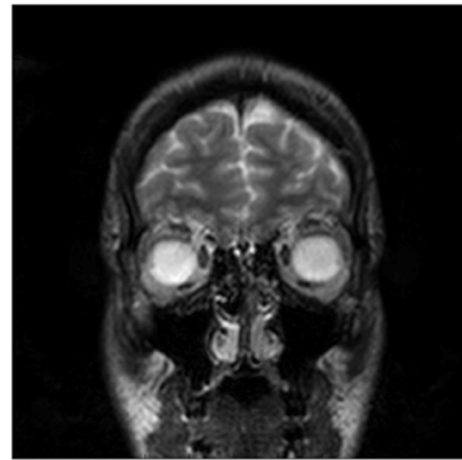
(c)
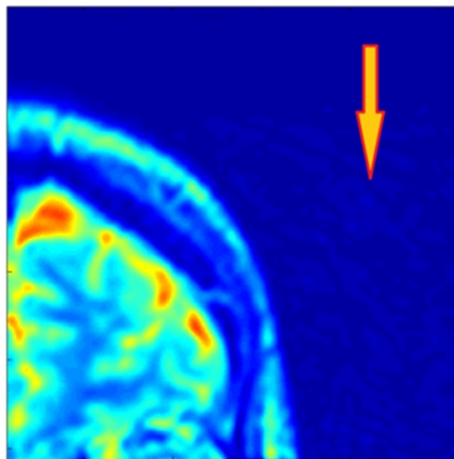
(d)
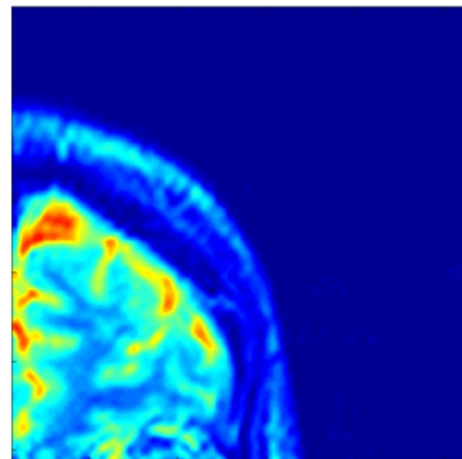
(e)

Figure 5.6: Sagittal T2 TSE head scan experiment image data. (a) SoS of absolute signal data from 32 channel; (b) MRI scanner's output using the mSENSE method; (c) the result of the SENSE method that uses calculated sensitivity map; (d) Magnified right part of image given in (b) and artifacts are marked with red arrows; (e) Magnified right part of image given in (c).

55
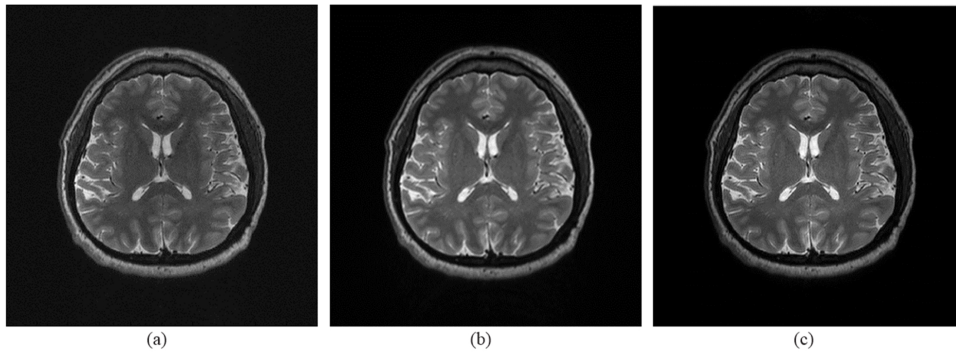
Figure 5.7: Without any acceleration the proposed method is used for the combination of each channels signal data. (a) SoS of absolute signal data from 32 channel; (b) MRI machines final output image; (c) Provided methods combination of 32 channel. In SoS construction coil inhomogeneity is clear (center of the image is darker than outside in (a). The machines result (b) and the proposed methods result (c) are similar and homogenous. MRI machine used pre-scan data for inhomogeneity correction but in (c) no additional acquisition data is used. Contrast and details are better in (c) than in (b) in all regions of the brain.
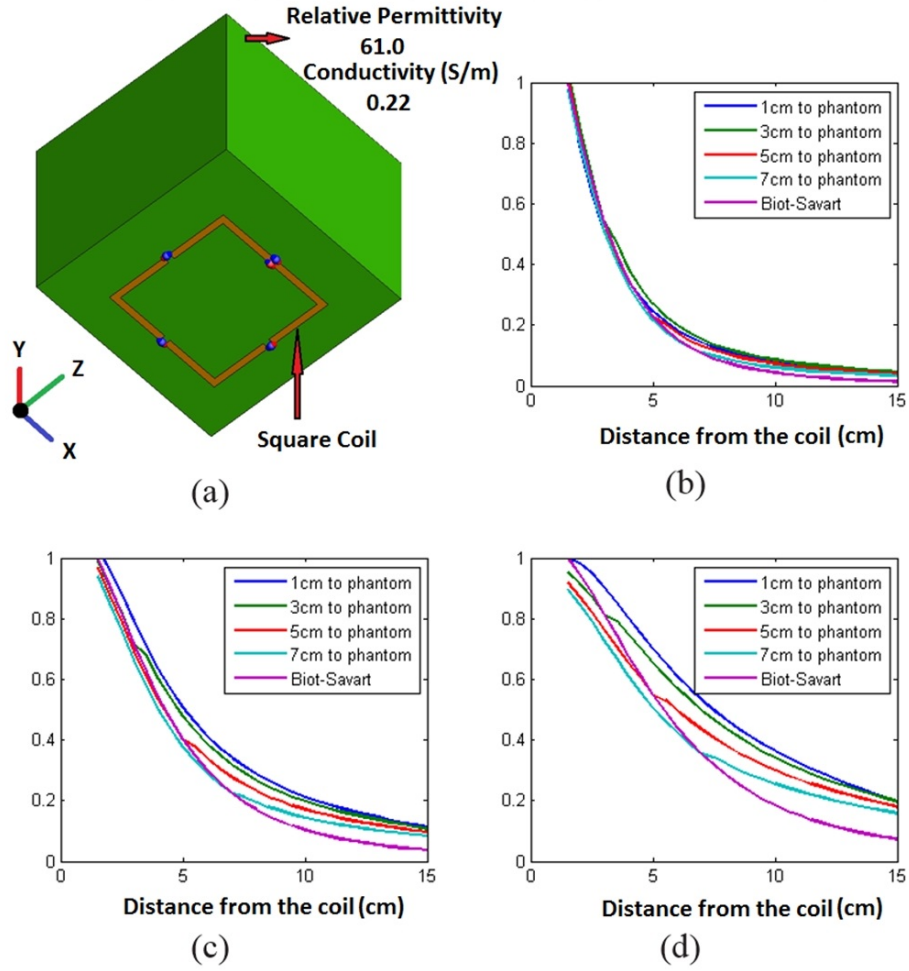
Figure 5.8: Electromagnetic simulation results for three different sized square coils with a phantom at 3 Tesla. An illustration of experimental setup and comparison of the simulated B_1^- magnitudes and the calculated Biot-Savart ones are given. (a) Figure of an experiment setup, a 200 mm x 200 mm x 200 mm cube phantom and a square shaped coil element is shown; (b) Normalized magnitude results of coil with side length of 6 cm; (c) Coil with side length of 9 cm results; (d) Coil with side length of 12 cm results.

CHAPTER 6

DISCUSSION

6.1 Evaluation of the Method and the Experiments

Various experiments have been carried out and the proposed method has been analyzed in different aspects both on real world images and on simulation data. According to the results of the real scan data, the proposed method produces consistent and satisfactory outputs in each scenario. In addition, experiments on the simulation tool show that the success of the proposed method depends heavily on the size of the coil.

In the proposed method, one of the most important steps was to determine the exact coil element positions in 3D imaging space. Since the head coil is fixed to the patient table in our head coil case, position and, thus, location of each coil element with respect to the image slices were calculated precisely. Moreover, it was seen that, in case of a miscalculation, quality of the reconstructed images decreases dramatically even with small errors (such as several mm). This indicates two important facts. One is that: our approach is correct (i.e. the coil sensitivities are very much related with the coil shape and its position with respect to the imaging region). The other is that the position calculation should be correct and in case of errors in the computation, the performance of proposed method will decrease accordingly.

As stated in Chapter 1, one of the main usage areas of the MRI is to image the internals of the head. Fortunately, most of the head coils are fixed to the patient tables and they are rigid. The exact coil shape can be obtained from the coil manufacturers as we did in this study. Using the coil shape and table position information, finding the location of each coil element relative to the image slice is relatively an easy task. The

calculation of coil sensitivity magnitude maps is not very time-consuming. More-over, they can be computed once and used anytime later. Once the coil sensitivity magnitude maps are calculated, they can be ready before an examination and after a position adjustment operation they can be used directly in each scan. As a result, post processing duration will not be affected because of the proposed method.

If the coil is not attached to the table or the coil position is not retrieved from the data provided by the machine, there are still several ways to get the coil position and orientation with respect to the MRI machine coordinate system. One possible and simple method is locating a number of markers inside the coil. Marker is an object which can be visualized easily from the MRI scanner. We have mentioned about oil pill markers in section 5.1 which we have utilized for finding our head coil position. For example, in our experiments, we used small fish oil pills since they can be seen as bright objects in the images. Vegetable oils can also be used as marker as stated in study [115]. We stuck at least 3 pills over the coil surface and by using the images containing pills, we could easily find the exact coil position. We made these experiments to verify the table information and our coil position calculation approach. Another possible method for determining the coil location is slightly complicated. Coil sensitivities change depending on the distance to the imaging object. Therefore, using such intensity changes in the images of the objects, coil positions can be estimated. In most of the phased-array coils, the channel positions are fixed relative to each other's. If one of the coil element position is found the others can be found trivially. In addition, from the estimations of each channel position, the exact coil location with respect to the imaged object can be found precisely. Since we were able to easily calculate our coil position from the MRI scan data, the second method mentioned in this paragraph is left as a future study.

If the sensitivity profiles are created on-line by using signal information which are collected during the scan or pre-scan, they can be easily affected from the spatial movements of patients during MRI examination. However, in the proposed method, we obtained the sensitivities of the coils directly from the shape information of the coils, i.e. our sensitivities are independent from the object scanned. Since the shape and the position of the coil (head coils are fixed to the patient table) does not change during the examinations, our calculated sensitivity profiles also do not change, since

they are independent from the object movements. For example, in our machine, the sensitivity profiles are found by division of body coil and the surface coil images which are collected during pre-scan phase of the examination process. However, if the scanned object position changes during the scan, the found sensitivities will not be correct. They are affected from the position changes and using these sensitivities in case of object movements will create artifacts in parallel imaging applications. Therefore, when compared to the methods using pre-scan, our method is more reliable in case of object movements.

In a previous study [86], Biot-Savart law was used for the enhancement of coil sensitivity maps on simulated data. In the study, *a priori* knowledge of approximate coil geometry was utilized and the sensitivity of the coils were refined using optimization processes. However, as in our head coil case, the coil elements do not have always basic shapes (i.e. circular, elliptical or rectangular) in real life. Therefore, it may not be possible to find the exact coil geometries from the raw sensitivity profiles and the proposed method in the study [86] cannot guarantee high performance on complex coil shapes. Moreover, as stated in the study, that method is applicable only in low fields ($B_0 \leq 1.5$ Tesla) and cannot be used in high fields. Furthermore, internal electrical properties of the object, which is being scanned, may cause unexpected consequences and may decrease the performance of such an approach.

With the advent of stronger magnets ($B_0 \geq 3$ Tesla) RF field's homogeneity becomes a serious problem. In order to make the transmit field homogeneous, RF shimming ([116]) can be used. However, coil sensitivities and body internals are the two most important factors to receive field homogeneity. The method we propose can be considered as an alternative technique for inhomogeneity correction. Coil sensitivity information can be used solely for the correction of intensity variations on the images as illustrated in Fig. 5.7. As shown in our experiments (shown in Fig. 5.4-5.6) the reconstructed images with the proposed method provide better results in terms of homogeneity. Detailed analysis of the homogeneity evaluations are explained in section 6.2.2.

As stated in [86], the known method for finding coil sensitivities is the division of the images constructed from the surface coil data with a known uniform reference

image which is usually obtained either from a body coil or SoS of all coil channel elements. However, such methods suffer from two main problems. First, in higher magnetic fields neither the body coil image nor the SoS of surface coil images are uniform. Second, division process accumulates additional errors especially in low proton density areas in the images [73], since the noise is augmented by division in these regions. Proposed solution for sensitivity mapping does not carry any proton density information, therefore it does not increase the level of noise. Moreover, in division approach the created sensitivity maps have lower resolution because most of the time, the reference images have lower resolution than the actual ones. Before the reconstruction process using interpolation techniques, the resolution of the sensitivities are equalized to the actual images. This process creates additional errors. However, in the proposed method, the resolution of the sensitivity maps are independent from the scan configuration. Therefore, much better resolution maps can be calculated easily. As seen in Fig. 5.4-5.7, the resolution and homogeneity of the final images are better in the proposed method than that of machine outputs.

In the proposed method, only the phase images of the reference low resolution signal data were used. Phase images are not affected as much as magnitude images from phase encoding line counts in the reference scans. Therefore, the total scan can be accelerated by decreasing the phase encoding lines in reference scans. Moreover, with further studies, phase images can be calculated without additional scan or pre-scan data, and thus, the time for the examination can be decreased. In such a case, since the sensitivity maps will be computed, artifacts due to usage of low resolution reference data in sensitivity estimations will be eliminated.

We assumed that each channel of the head coil is perfectly tuned and there is no coupling between elements. Even though the load (head or phantom) effect was taken into account in phase values of sensitivity maps, it was ignored in magnitude values. When the results of the experiments are analyzed, our method is found to be successful in 32 channel head coil. This means that the assumptions made in this study did not create a noticeable problem in reconstruction. Actually, our results are better than the machine outputs in several aspects (such as it generates higher resolution maps and therefore images with better fine details, decreases artifact level significantly and provides more homogeneous images). Detailed quality analysis is given in section

6.2.1.

There are several studies [117, 118] about load effect on RF fields. These studies showed that the dielectric media (tissue or phantom) alters the wave propagation compared to air/free-space in high fields ($B_0 \geq 3$ Tesla). This concurs with our simulation results shown in Fig. 5.8. However, the difference between the actual magnitude values and Biot-Savart law results get smaller as the coil size decreases. The effect of coil to phantom distance is shown in panel (b-d) of Fig. 5.8. It is seen that when the electromagnetic wave propagates from one medium (air) to another (phantom), the wave bends but the rate of decrease in magnitude does not change significantly between different mediums (tissues of the head) for small coils. In a recent study [119], a lossy multi-layered spherical head phantom which has similar radial conductivity and permeability profiles as human head was designed. RF field behavior in the human head was analyzed both with surface and volume coils. In that study, various coil sizes (6 cm - 10 cm radii) in different distances (0.5 cm - 4 cm) to the model were tested and magnetic, electric field, specific absorption rate (SAR) pattern and loss resistance characteristics were measured for each case. Our results are in accordance with this study; loss resistance increases with RF frequency and the radii of the coil, and decreases with coil to phantom distance.

As stated in the study [106], RF wavelength on average for in vivo brain imaging is 27 cm. Our head coil internal size where human head places has a diameter of about 22 cm. A typical human head is even smaller than these sizes as the head coil is commercial and used in many hospitals. Typical human sizes are given in the study [104]. In addition, as stated in the study [120], as the coil size decreases the region where the coil collects signal also decreases. In surface coils, sensitivity drops off very rapidly as a function of distance from the coil. Therefore, as in our head coil, the effective region where the coil collects the signal is half the head size, which is much shorter than the RF wavelength at that magnetic field strength.

We have also given our simulation results and shown how the load affects the sensitivity profile. In the simulations, the simulated coil is tuned for 3 cm distance between imaging object and the coil. As the coil size decreases, the sensitivity profiles get closer to the Biot-Savart law results (Fig. 5.8). In the simulation, we have also

demonstrated how the loaded object and its distance to the coil affects the sensitivity profiles. In addition, we have tested our method in phantom and on several volunteers which have different head sizes. We have also carried out experiments on volunteers. One of our volunteers had a head periphery about 8 cm shorter than another volunteer. In all experiments on volunteers, even though their head sizes differs significantly, we obtained better results when compared to the machine's output.

We prove with our experiments that if the coil gets smaller, the sensitivity profiles get closer to the calculated ones as our approach proposes. The effects of load (body) or the movements during the scan did not create a significant problem in our experiments. It does not mean that tuning, load, or movement problems do not affect the performance of the sensitivity approaches, but these problems create lower effects on our approach as our method produces better quality images. In addition, the effects of these problems get minor as the coil size decreases. This is also stated in study [106] as the magnitude of the magnetic field variations due to load (body) can be ignored for coil elements.

As a conclusion, our analysis and previous studies show that if the coil size is small and there is no other significant error source (i.e. coil tuning is nearly optimal and coupling effect among the elements is ignorable), the proposed method can be used for parallel image reconstruction and intensity correction in the images. Proposed method has produced successful results using a commercial 32 channel head coil. We believe that, after further studies (i.e. usefulness of the proposed method will be tested under different settings and on other small coils available in the market), our method can be improved and may be ready to be used in practice. In such a case, the future coil designs will also be affected from the proposed method.

6.2 Evaluation of Resulted Images

We have evaluated the results of our method in terms of:

- Image quality

- Image homogeneity

64

6.2.1 Image quality

There are several approaches on the evaluation of image qualities in the literature. However, almost all of them require a reference image. The qualities of the methods are quantified by comparing the similarities between the result and the reference image. That is, the method which produces the most similar image to the reference image is categorized as the most successful method. As the similarity distance between the reference image and the compared image decrease, the success of the method increases. Thus, the quality of an image processing method is quantified in this way. However, in our study, since we worked on real volunteer head images, we did not have any reference image. Therefore, we could not compare our result with the machine's result over a reference image. Instead, for the evaluation of the results we conducted a survey on domain experts. A group of experts (2 radiologists, a neurologist, 2 expert doctors and 9 professionals working on medical image processing) analyzed our results of more than 20 MRI images and compared the outputs generated by the machine and those obtained by the proposed method.

We prepared a questionnaire for our domain experts in order to compare the results in terms of image quality parameters: resolution, sharpness, artifact level, homogeneity and contrast. 14 of the experts preferred the results we obtained for having better resolution, sharpness, and low level of artifact. 9 experts, including the radiologists and a neurologist, found the quality increase significant. 6 of 9 the experts selected our method as providing improved contrast and the other 8 experts reported that the contrast is similar in both methods.

In order to make a quantitative quality assessment we used Signal to Noise Ratio (SNR) in the images. For this, we used the following formula (Eg. 6.1).

$$SNR = \frac{SOR}{SOOR} \tag{6.1}$$

In Eg. 6.1, SOR refers to the **pixel value sum of the object region** and $SOOR$ refers to the **pixel value sum of the region outside of the object**. For a good imaging we anticipate no signal outside of the imaging object, as any value outside of the image is accepted as noise. If we accept the signal as the total pixel values of imaging object,

and noise as the total pixel values outside this object then we can easily calculate SNR using the Eg. 6.1.

We calculated signal to noise ratio (SNR) values by using Eg. 6.1 for all images and our method provided at least 11% better SNR values for all cases. Moreover, in all of the images, our method generates less signal outside the imagining object.

6.2.2 Image homogeneity

It is expected to get homogeneous images (i.e. signal intensity level should be similar over same tissue or same material like phantom) in an MR image and in uniform phantom MR images. For this purpose, we have tested the intensity changes over uniform phantom images and compared the results with the machine's output. In accelerated scans of those images, especially over the folded parts, the intensity differences are about 10% in the machine's method and about 1% in our proposed method. In addition, MRI machine promises homogeneity using pre-scan data. In normal (not accelerated) scans, the intensity difference over the object pixels between the images generated by the machine and our method is less than 3%. This shows that homogeneity characteristics between our method and the machine's software is similar.

An example is given for comparison in Fig. 6.1. In the figure, SoS construction is shown in panel (a). It is not homogeneous since the middle part has a lower signal level when compared to the outer parts of the head. As shown with arrow in (d), center of the image is not in similar in color when compared with the images in (e) and (f). This is not expected for the tissue in the middle of head, which has to be red as in (e) and (f). As it is shown in the third row, (h) and (i) have similar homogeneity characteristics, but in (g) middle region has smaller values. Moreover, in third row in Fig. 6.1, red arrows show signal levels outside the imaging object. In graph (i) noise is much smaller when compared to the other two graphs in (g) and (h). This shows that our method produces much smaller noise when compared to the other methods. Signal intensity in the middle part of the graph in panel (i) is much higher when compared to the other parts in the graph. But in graph (h), the middle part in the graph is a little bit smaller. According to the MRI machine's vendor, inhomogeneity correction in higher fields using pre-scan data causes a decrease in signal level the

middle regions (i.e. that parts away from the body coil). However, as it is seen in graph (i), our approach does not have this problem.

Thus, MRI machine uses pre-scan data for inhomogeneity correction but in our method we do not use any additional acquisition data. In addition, it is clear in Fig. 6.1 that our method provides the best image in terms of sharpness, noise level and contrast. All of the domain experts had the same opinion.
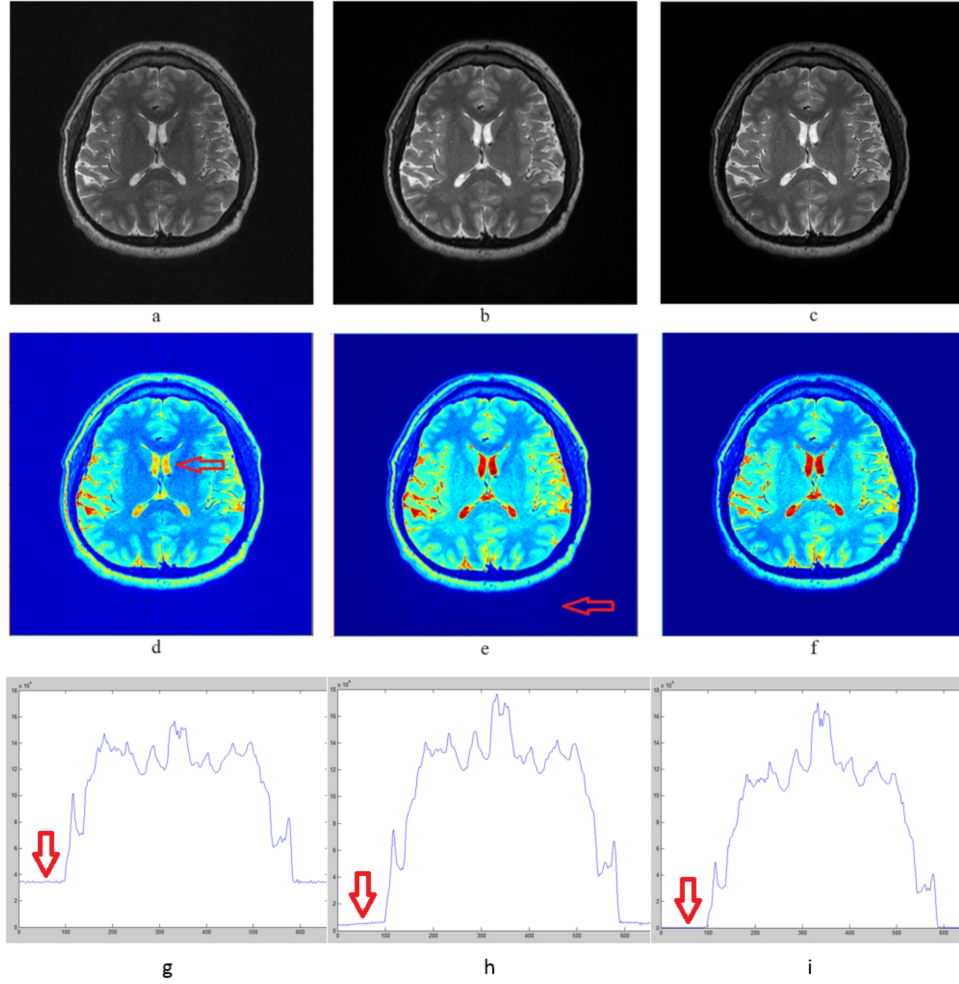
Figure 6.1: Out puts of a scan without acceleration. Each channels signal data is combined with different methods. (a) SoS of absolute signal data from 32 channel; (b) MRI machines output image; (c) Our methods combination. Second row images: (d), (e) and (f) are the jet colored images of the gray scale (a), (b) and (c) respectively. In this set red arrows show the signal values outside the object regions. Third row images: (g), (h) and (i) are the pixel value sums in vertical direction of images in (a), (b) and (c) respectively.

CHAPTER 7

CONCLUSION AND FUTURE WORK

Currently, MRI machines contain one of the most advanced imaging technologies in medicine. Without any doubt, human life has the greatest importance and this machine is used for increasing the lifespan and life quality of human-beings. It provides superior contrast and better resolution images of body internals when compared to the other medical imaging devices like CT, X-Ray, Thermography or Ultrasound.

Besides the imaging capabilities solely on the content of the body internals, an MRI machine can be used for other crucial purposes. For example, using fMRI [28] procedurei the machine can visualize the cell activities and give useful information about functional behaviors of body cells, especially the neuron cells. Moreover, with MRI Spectroscopy [29, 121], MRI machine can identify various metabolites and find their concentrations in a region of interest inside the body.

Because of its numerous capabilities, MRI machine has a great number of application areas and can be used for several medical purposes like the diagnostics and staging of cancer illness, identifying neurological problems, heart diseases, etc.

Since MRI is a very important technique used for medical purposes, there are great number of studies conducted by scientists. As scientists from different parts of the world are working in this area, we also aimed to further improve the capabilities of MRI machines. We believe that with this study, we made an enhancement in the capabilities of the MRI machine, and this study will open a new area of research for future studies.

This study focused mainly on coil spatial sensitivities, where a novel method is pro-

posed to calculate complex-valued coil spatial sensitivities at 3 Tesla. It has been applied to various setups on 7 volunteers and a phantom using a commercial 32 channel head coil. Moreover, the superior performance of the proposed approach is supported with simulations on an electromagnetic simulation software. It has been shown that, using this method, the images can be reconstructed using one of the known parallel imaging techniques (such as SENSE).

The results were examined by domain experts and medical doctors. According to them, the results of the experiments on volunteers and the phantom, our approach generated more uniform images with better resolution and less artifacts compared to the sensitivity maps obtained using low resolution full k-space data. Thus, this method increased the image quality significantly as shown in Fig. 5.4-5.7. We also showed that it can be used solely for intensity correction purposes without losing diagnostic quality of the images. Moreover, as stated in the discussion chapter, our method has some limitations, but they can be eliminated with future studies.

REFERENCES

[1] Siemens Healthcare USA. 32-channel head coil. `https://usa.healthcare.siemens.com/magnetic-resonance-imaging/options-and-upgrades/coils/32-channel-head-coil`, Accessed: 01 Jan 2015.

[2] Ray Hashman Hashemi, William G Bradley, and Christopher J Lisanti. *MRI: the basics*. Lippincott Williams & Wilkins, 2012.

[3] Kieran Maher and Wikibooks Contributors. *Basic physics of nuclear medicine*. Libronomia Company, 2006.

[4] Harald T Lutz and Hassen A Gharbi. *Manual of diagnostic ultrasound in infectious tropical diseases*, volume 218. Springer Science & Business Media, 2005.

[5] Vincent Chan and Anahi Perlas. Basics of ultrasound imaging. In *Atlas of ultrasound-guided procedures in interventional pain management*, pages 13–19. Springer, 2011.

[6] Jonathan Ophir, Ignacio Cespedes, Hm Ponnekanti, Y Yazdi, and Xin Li. Elastography: a quantitative method for imaging the elasticity of biological tissues. *Ultrasonic imaging*, 13(2):111–134, 1991.

[7] Parris Saxon Wellman. *Tactile imaging*. PhD thesis, Harvard University, 1999.

[8] Minghua Xu and Lihong V Wang. Photoacoustic imaging in biomedicine. *Review of scientific instruments*, 77(4):041101, 2006.

[9] Tracy A Turner. Diagnostic thermography. *The Veterinary clinics of North America. Equine practice*, 17(1):95–113, 2001.

[10] BB Lahiri, S Bagavathiappan, T Jayakumar, and John Philip. Medical applications of infrared thermography: a review. *Infrared Physics & Technology*, 55(4):221–235, 2012.

[11] Mary Diakides, Joseph D Bronzino, and Donald R Peterson. *Medical Infrared Imaging: Principles and Practices*. CRC press, 2012.

[12] J Gershon-Cohen, JA Haberman-Brueschke, and EE Brueschke. Medical thermography: a summary of current status. *Radiologic clinics of North America*, 3(3):403, 1965.

[13] Kazuhiko Atsumi. *Medical thermography*. Columbia Univ Pr, 1973.

[14] Jiang Hsieh. Computed tomography: principles, design, artifacts, and recent advances. SPIE Bellingham, WA, 2009.

[15] Dale L Bailey, David W Townsend, Peter E Valk, and Michael N Maisey. *Positron emission tomography*. Springer, 2005.

[16] Simon R Arridge. Optical tomography in medical imaging. *Inverse problems*, 15(2):R41, 1999.

[17] Catherine M Otto. *The practice of clinical echocardiography*. Elsevier Health Sciences, 2012.

[18] Scott C Bunce, Meltem Izzetoglu, Kurtulus Izzetoglu, Banu Onaral, and Kambiz Pourrezaei. Functional near-infrared spectroscopy. *Engineering in Medicine and Biology Magazine, IEEE*, 25(4):54–62, 2006.

[19] Arno Villringer, J Planck, C Hock, L Schleinkofer, and U Dirnagl. Near infrared spectroscopy (nirs): a new tool to study hemodynamic changes during activation of brain function in human adults. *Neuroscience letters*, 154(1):101–104, 1993.

[20] Main Line Health. Magnetic resonance imaging (mri): Main line health, philadelphia, pennsylvania. `http://www.mainlinehealth.org/imaging/procedures/mri`, Accessed: 01 Jan 2015.

[21] Valentina Hartwig, Giulio Giovannetti, Nicola Vanello, Massimo Lombardi, Luigi Landini, and Silvana Simi. Biological effects and safety in magnetic resonance imaging: a review. *International journal of environmental research and public health*, 6(6):1778–1798, 2009.

[22] Stuart W Young. Magnetic resonance imaging: basic principles. 1987.

[23] Robert W Brown, Y-C Norman Cheng, E Mark Haacke, Michael R Thompson, and Ramesh Venkatesan. *Magnetic resonance imaging: physical principles and sequence design*. John Wiley & Sons, 2014.

[24] Zhi-Pei "" Liang and Paul C Lauterbur. *Principles of magnetic resonance imaging: a signal processing perspective*. "The" Institute of Electrical and Electronics Engineers Press, 2000.

[25] Peter G Morris. *Nuclear magnetic resonance imaging in medicine and biology*. Clarendon Press, 1986.

[26] Ann L Scherzinger and William R Hendee. Basic principles of magnetic resonance imaging—an update. *Western Journal of Medicine*, 143(6):782, 1985.

[27] Charles P Slichter. *Principles of magnetic resonance*, volume 1. Springer Science & Business Media, 2013.

[28] Chrit TW Moonen and Peter A Bandettini. *Functional mri*. Boom Koninklijke Uitgevers, 2000.

[29] Robin Kingsley Harris. Nuclear magnetic resonance spectroscopy. 1986.

[30] Lloyd Miles Jackman and Sever Sternhell. *Application of Nuclear Magnetic Resonance Spectroscopy in Organic Chemistry: International Series in Organic Chemistry*. Elsevier, 2013.

[31] WebMD. Magnetic resonance imaging (mri). `http://www.webmd.com/a-to-z-guides/magnetic-resonance-imaging-mri`, Accessed: 01 July 2015.

[32] John F Schenck. Health and physiological effects of human exposure to whole-body four-tesla magnetic fields during mri. *Annals of the New York Academy of Sciences*, 649(1):285–301, 1992.

[33] Domenico Formica and Sergio Silvestri. Biological effects of exposure to magnetic resonance imaging: an overview. *Biomedical engineering online*, 3(1):11, 2004.

[34] John F Schenck. Safety of strong, static magnetic fields. *Journal of magnetic resonance imaging*, 12(1):2–19, 2000.

[35] Peter Kellman. Parallel imaging: the basics. *ISMRM Educational Course: MR physics for physicists*, 2004.

[36] Block Imaging. Advantages of phased array mri coils. `http://info.blockimaging.com/bid/84437/Advantages-of-Phased-Array-MRI-Coils`, Accessed: 01 July 2015.

[37] Anagha Deshmane, Vikas Gulani, Mark A Griswold, and Nicole Seiberlich. Parallel mr imaging. *Journal of Magnetic Resonance Imaging*, 36(1):55–72, 2012.

[38] Klaas P Pruessmann, Markus Weiger, Markus B Scheidegger, Peter Boesiger, et al. Sense: sensitivity encoding for fast mri. *Magnetic resonance in medicine*, 42(5):952–962, 1999.

[39] Mark A Griswold, Peter M Jakob, Robin M Heidemann, Mathias Nittka, Vladimir Jellus, Jianmin Wang, Berthold Kiefer, and Axel Haase. Generalized autocalibrating partially parallel acquisitions (grappa). *Magnetic Resonance in Medicine*, 47(6):1202–1210, 2002.

[40] Lars G Hanson. Introduction to magnetic resonance imaging techniques. 2009.

[41] E Mark Haacke, Robert W Brown, Michael R Thompson, Ramesh Venkatesan, et al. *Magnetic resonance imaging: physical principles and sequence design*, volume 82. Wiley-Liss New York:, 1999.

[42] Michael Hutchinson and Ulrich Raff. Fast mri data acquisition using multiple detectors. *Magnetic resonance in Medicine*, 6(1):87–91, 1988.

[43] Joseph W Carlson. An algorithm for nmr imaging reconstruction based on multiple rf receiver coils. *Journal of Magnetic Resonance (1969)*, 74(2):376–380, 1987.

[44] Peter B Roemer, William A Edelstein, Cecil E Hayes, Steven P Souza, and OM Mueller. The nmr phased array. *Magnetic resonance in medicine*, 16(2):192–225, 1990.

[45] Eli Brookner. Phased-array radars. *Scientific American*, 252(2):94–102, 1985.

[46] Robert C Hansen. *Phased array antennas*, volume 213. John Wiley & Sons, 2009.

[47] Paul F McManamon, Terry A Dorschner, David L Corkum, Larry J Friedman, Douglas S Hobbs, Michael Holz, Sergey Liberman, Huy Q Nguyen, Daniel P Resler, Richard C Sharp, et al. Optical phased array technology. *Proceedings of the IEEE*, 84(2):268–298, 1996.

[48] Rainer Kronberger, Thomas Knie, Roberto Leonardi, Uwe Dettmar, Markus Cremer, and Salah Azzouzi. Uhf rfid localization system based on a phased array antenna. In *Antennas and Propagation (APSURSI), 2011 IEEE International Symposium on*, pages 525–528. IEEE, 2011.

[49] OT VonRamm and FL Thurstone. Cardiac imaging using a phased array ultrasound system. i. system design. *Circulation*, 53(2):258–262, 1976.

[50] Martin Uecker. Parallel magnetic resonance imaging. *arXiv preprint arXiv:1501.06209*, 2015.

[51] D Kwiat, S Einav, and G Navon. A decoupled coil detector array for fast image acquisition in magnetic resonance imaging. *Medical physics*, 18(2):251–265, 1991.

[52] JW Carlson and T Minemura. Imaging time reduction through multiple receiver coil data acquisition and image reconstruction. *Magnetic resonance in medicine*, 29(5):681–687, 1993.

[53] JB Ra and CY Rim. Fast imaging using subencoding data sets from multiple detectors. *Magnetic resonance in medicine*, 30(1):142–145, 1993.

[54] Daniel K Sodickson and Warren J Manning. Simultaneous acquisition of spatial harmonics (smash): fast imaging with radiofrequency coil arrays. *Magnetic Resonance in Medicine*, 38(4):591–603, 1997.

[55] Mark A Griswold, Peter M Jakob, Mathias Nittka, James W Goldfarb, and Axel Haase. Partially parallel imaging with localized sensitivities (pils). *Magnetic Resonance in Medicine*, 44(4):602–609, 2000.

[56] Martin Blaimer, Felix Breuer, Matthias Mueller, Robin M Heidemann, Mark A Griswold, and Peter M Jakob. Smash, sense, pils, grappa: how to choose the optimal method. *Topics in Magnetic Resonance Imaging*, 15(4):223–236, 2004.

[57] Peng Qu, Jing Luo, Bida Zhang, Jianmin Wang, and Gary X Shen. An improved iterative sense reconstruction method. *Concepts in Magnetic Resonance Part B: Magnetic Resonance Engineering*, 31(1):44–50, 2007.

[58] J Wang, T Kluge, M Nittka, V Jellus, B Kuehn, and B Kiefer. Parallel acquisition techniques with modified sense reconstruction msense. In *Proceedings of the First Würzburg Workshop on Parallel Imaging Basics and Clinical Applications*, 2001.

[59] Jianmin Wang, Thomas Kluge, Mathias Nittka, Vladimir Jellus, Bernd Kuhn, and Berthold Kiefer. Using reference lines to improve the snr of msense. In *Proceedings of the 10th Annual Meeting of ISMRM, Honolulu*, page 2392, 2002.

[60] Leslie Ying, Bo Liu, Michael C Steckner, Gaohong Wu, Min Wu, and Shi-Jiang Li. A statistical approach to sense regularization with arbitrary k-space trajectories. *Magnetic Resonance in Medicine*, 60(2):414–421, 2008.

[61] Dong Liang, Bo Liu, JiunJie Wang, and Leslie Ying. Accelerating sense using compressed sensing. *Magnetic Resonance in Medicine*, 62(6):1574–1584, 2009.

[62] Bo Liu, Kevin King, Michael Steckner, Jun Xie, Jinhua Sheng, and Leslie Ying. Regularized sensitivity encoding (sense) reconstruction using bregman iterations. *Magnetic Resonance in Medicine*, 61(1):145–152, 2009.

[63] Ya-Jun Ma, Wentao Liu, Xin Tang, and Jia-Hong Gao. Improved sense imaging using accurate coil sensitivity maps generated by a global magnitude-phase fitting method. *Magnetic Resonance in Medicine*, 2014.

[64] Peter M Jakob, Mark A Grisowld, Robert R Edelman, and Daniel K Sodickson. Auto-smash: a self-calibrating technique for smash imaging. *Magnetic Resonance Materials in Physics, Biology and Medicine*, 7(1):42–54, 1998.

[65] Robin M Heidemann, Mark A Griswold, Axel Haase, and Peter M Jakob. Vd-auto-smash imaging. *Magnetic Resonance in Medicine*, 45(6):1066–1074, 2001.

[66] Mark Bydder, David J Larkman, and Joseph V Hajnal. Generalized smash imaging. *Magnetic resonance in medicine*, 47(1):160–170, 2002.

[67] Feng Huang, James Akao, Sathya Vijayakumar, George R Duensing, and Mark Limkeman. k-t grappa: A k-space implementation for dynamic mri with high reduction factor. *Magnetic Resonance in Medicine*, 54(5):1172–1184, 2005.

[68] Bernd J Wintersperger, Konstantin Nikolaou, Olaf Dietrich, Johannes Rieber, Matthias Nittka, Maximilian F Reiser, and Stefan O Schoenberg. Single breath-hold real-time cine mr imaging: improved temporal resolution using generalized autocalibrating partially parallel acquisition (grappa) algorithm. *European radiology*, 13(8):1931–1936, 2003.

[69] Felix A Breuer, Peter Kellman, Mark A Griswold, and Peter M Jakob. Dynamic autocalibrated parallel imaging using temporal grappa (tgrappa). *Magnetic Resonance in Medicine*, 53(4):981–985, 2005.

[70] Yu Ding, Yiu-Cho Chung, Mihaela Jekic, and Orlando P Simonetti. A new approach to autocalibrated dynamic parallel imaging based on the karhunen-loeve transform: Kl-tsense and kl-tgrappa. *Magnetic Resonance in Medicine*, 65(6):1786–1792, 2011.

[71] Martin Uecker, Peng Lai, Mark J Murphy, Patrick Virtue, Michael Elad, John M Pauly, Shreyas S Vasanawala, and Michael Lustig. Espirit—an eigenvalue approach to autocalibrating parallel mri: where sense meets grappa. *Magnetic Resonance in Medicine*, 71(3):990–1001, 2014.

[72] Robin M Heidemann, Özkan Özsarlak, Paul M Parizel, Johan Michiels, Berthold Kiefer, Vladimir Jellus, Mathias Müller, Felix Breuer, Martin Blaimer, Mark A Griswold, et al. A brief review of parallel magnetic resonance imaging. *European radiology*, 13(10):2323–2337, 2003.

[73] Mark A Griswold, Felix Breuer, Martin Blaimer, Stephan Kannengiesser, Robin M Heidemann, Matthias Mueller, Mathias Nittka, Vladimir Jellus, Berthold Kiefer, and Peter M Jakob. Autocalibrated coil sensitivity estimation for parallel imaging. *NMR in Biomedicine*, 19(3):316–324, 2006.

[74] Klaas P Pruessmann, Markus Weiger, Peter Börnert, and Peter Boesiger. Advances in sensitivity encoding with arbitrary k-space trajectories. *Magnetic Resonance in Medicine*, 46(4):638–651, 2001.

[75] Daniel K Sodickson. Tailored smash image reconstructions for robust in vivo parallel mr imaging. *Magnetic resonance in medicine*, 44(2):243–251, 2000.

[76] David O Walsh, Arthur F Gmitro, and Michael W Marcellin. Adaptive reconstruction of phased array mr imagery. *Magnetic Resonance in Medicine*, 43(5):682–690, 2000.

[77] Mark A Griswold, David Walsh, Robin M Heidemann, Axel Haase, and Peter M Jakob. The use of an adaptive reconstruction for array coil sensitivity mapping and intensity normalization. 2002.

[78] FH Lin, KK Kwong, YJ Chen, JW Belliveau, and LL Wald. Reconstruction of sensitivity encoded images using regularization and discrete time wavelet transform estimates of the coil maps. In *Proceedings of the 10th Annual Meeting of ISMRM, Honolulu, HI, USA*, page 2389, 2002.

[79] ZP Liang, R Bammer, J Ji, NJ Pelc, and GH Glover. Making better sense: wavelet denoising, tikhonov regularization, and total least squares. *International Society for Magnetic Resonance in Medicine, Hawaı, USA*, 2388, 2002.

[80] Michael Lustig, David Donoho, and John M Pauly. Sparse mri: The application of compressed sensing for rapid mr imaging. *Magnetic resonance in medicine*, 58(6):1182–1195, 2007.

[81] Charles A McKenzie, Ernest N Yeh, Michael A Ohliger, Mark D Price, and Daniel K Sodickson. Self-calibrating parallel imaging with automatic coil sensitivity extraction. *Magnetic Resonance in Medicine*, 47(3):529–538, 2002.

[82] Albert L Baert and Daniela Prayer. *Fetal MRI*. Springer, 2011.

[83] Klaas P Pruessmann. Encoding and reconstruction in parallel mri. *NMR in Biomedicine*, 19(3):288–299, 2006.

[84] Peter Kellman, Frederick H Epstein, and Elliot R McVeigh. Adaptive sensitivity encoding incorporating temporal filtering (tsense)†. *Magnetic Resonance in Medicine*, 45(5):846–852, 2001.

[85] XiaoFang Liu, Xiuzi Ye, Sanyuan Zhang, and Feng Liu. Regularized least squares estimating sensitivity for self-calibrating parallel imaging. *Journal of Computers*, 6(5):857–864, 2011.

[86] Jin Jin, Feng Liu, Ewald Weber, Yu Li, and Stuart Crozier. An electromagnetic reverse method of coil sensitivity mapping for parallel mri–theoretical framework. *Journal of Magnetic Resonance*, 207(1):59–68, 2010.

[87] Radiopaedia. Gibbs and truncation artifacts. `http://radiopaedia.org/articles/gibbs-and-truncation-artifacts`, Accessed: 01 July 2015.

[88] IMV. *MRI Market Benchmark Report*. Information for the decision ahead, 2010.

[89] William G Bradley, Michael Brant-Zawadski, and Jane Cambray-Forker. *MRI of the Brain*, volume 1. Lippincott Williams & Wilkins, 2001.

[90] RadiologyInfo. Head mri (magnetic resonance imaging). `http://www.radiologyinfo.org/en/info.cfm?pg=headmr`, October 2015.

[91] Joseph P Hornak. Basics of nmr, 1997.

[92] Ralf Deichmann, CD Good, and Robert Turner. Rf inhomogeneity compensation in structural brain imaging. *Magnetic Resonance in medicine*, 47(2):398–402, 2002.

[93] Hiroaki Mihara, Norio Iriguchi, and Shogo Ueno. A method of rf inhomogeneity correction in mr imaging. *Magnetic Resonance Materials in Physics, Biology and Medicine*, 7(2):115–120, 1998.

[94] G Collewet, A Davenel, C Toussaint, and S Akoka. Correction of intensity nonuniformity in spin-echo t 1-weighted images. *Magnetic resonance imaging*, 20(4):365–373, 2002.

[95] Mark S Cohen, Richard M DuBois, and Michael M Zeineh. Rapid and effective correction of rf inhomogeneity for high field magnetic resonance imaging. *Human brain mapping*, 10(4):204–211, 2000.

[96] Bradley P Sutton, Douglas C Noll, and Jeffrey A Fessler. Fast, iterative image reconstruction for mri in the presence of field inhomogeneities. *Medical Imaging, IEEE Transactions on*, 22(2):178–188, 2003.

[97] Zujun Hou. A review on mr image intensity inhomogeneity correction. *International Journal of Biomedical Imaging*, 2006, 2006.

[98] Boubakeur Belaroussi, Julien Milles, Sabin Carme, Yue Min Zhu, and Hugues Benoit-Cattin. Intensity non-uniformity correction in mri: existing methods and their validation. *Medical Image Analysis*, 10(2):234–246, 2006.

[99] James B Arnold, Jeih-San Liow, Kirt A Schaper, Joshua J Stern, John G Sled, David W Shattuck, Andrew J Worth, Mark S Cohen, Richard M Leahy, John C Mazziotta, et al. Qualitative and quantitative evaluation of six algorithms for correcting intensity nonuniformity effects. *NeuroImage*, 13(5):931–943, 2001.

[100] Uros Vovk, Franjo Pernus, and Bostjan Likar. A review of methods for correction of intensity inhomogeneity in mri. *Medical Imaging, IEEE Transactions on*, 26(3):405–421, 2007.

[101] Magnetic Resonance Technology Information Portal. B1. `http://www.mr-tip.com/serv1.php?type=db1&dbs=B1`, October 2015.

[102] Pierre-Marie Robitaille and Lawrence Berliner. *Ultra high field magnetic resonance imaging*, volume 26. Springer Science & Business Media, 2007.

78

[103] Florian Wiesinger, Van de Moortele, Gregor Adriany, Nicola De Zanche, Kamil Ugurbil, Klaas P Pruessmann, et al. Potential and feasibility of parallel mri at high field. *NMR in Biomedicine*, 19(3):368–378, 2006.

[104] A Poston. Human engineering design data digest: human factors standardization systems. *Human Factors Standardization SubTAG*, 2000.

[105] Jin-hee Lee, Shin Hwang, Cynthia L Istook, et al. Analysis of human head shapes in the united states. *International Journal of Human Ecology*, 7(1):77–83, 2006.

[106] Sami Gabriel, RW Lau, and Camelia Gabriel. The dielectric properties of biological tissues: Iii. parametric models for the dielectric spectrum of tissues. *Physics in medicine and biology*, 41(11):2271, 1996.

[107] Peter Vaughan Elsmere McClintock. Essentials of in vivo biomedical imaging. *Contemporary Physics*, 57(1):144–145, 2016.

[108] Lawrence S Lerner. *Physics for Scientists and Engineers, Volume 2*. Jones & Bartlett Learning, 1997.

[109] James A Bankson and Steven M Wright. Simulation-based investigation of partially parallel imaging with a linear array at high accelerations. *Magnetic resonance in medicine*, 47(4):777–786, 2002.

[110] Ihab R Kamel and Elmar M Merkle. *Body MR imaging at 3 Tesla*. Cambridge University Press, 2011.

[111] Siemens Healthcare Global. Magnetom trio, a tim system 3t. `http://www.healthcare.siemens.com/magnetic-resonance-imaging/for-installed-base-business-only-do-not-publish/magnetom-trio-tim`, October 2015.

[112] Evangelia Kaza, Uwe Klose, and Martin Lotze. Comparison of a 32-channel with a 12-channel head coil: Are there relevant improvements for functional imaging? *Journal of Magnetic Resonance Imaging*, 34(1):173–183, 2011.

[113] Yudong Zhang, Bradley S Peterson, and Zhengchao Dong. A support-based reconstruction for sense mri. *Sensors*, 13(4):4029–4040, 2013.

[114] Altair. Feko - em simulation software. `https://www.feko.info/`, October 2015.

[115] Peter Pokieser, Ewald Schober, Karl Hittmair, Joachim Kettenbach, Jonathan Naudé, Friedrich Herbst, Judith Karner-Hanusch, Rudolf Segel, Herwig Imhof, and Josef Kramer. Vegetable oil as an mr contrast agent for rectal applications. *Magnetic resonance imaging*, 13(7):979–984, 1995.

[116] Michael B. Smith Mao, Weihua and Christopher M. Collins. Exploring the limits of rf shimming for highfield mri of the human head. *Magnetic resonance in medicine*, 56(4):918–922, 2006.

[117] Qing X Yang, Jinghua Wang, Xiaoliang Zhang, Christopher M Collins, Michael B Smith, Haiying Liu, Xiao-Hong Zhu, J Thomas Vaughan, Kamil Ugurbil, and Wei Chen. Analysis of wave behavior in lossy dielectric samples at high field. *Magnetic resonance in medicine*, 47(5):982–989, 2002.

[118] Tamer S Ibrahim, Chad Mitchell, Petra Schmalbrock, Robert Lee, and Donald W Chakeres. Electromagnetic perspective on the operation of rf coils at 1.5–11.7 tesla. *Magnetic resonance in medicine*, 54(3):683–690, 2005.

[119] Bin Xu, Bing Keong Li, Stuart Crozier, Qing Wei, and Feng Liu. Model implementation and case study for the lossy, multilayered spherical head phantom in mri application. In *Engineering in Medicine and Biology Society, 2005. IEEE-EMBS 2005. 27th Annual International Conference of the*, pages 1400–1403. IEEE, 2006.

[120] Jinyi Qi Simon R. Cherry, Ramsey D. Badawi. *Essentials Of In Vivo Biomedical Imaging*. CRC Press, 2015.

[121] Raymond John Abraham, Julie Fisher, and Philip Loftus. *Introduction to NMR spectroscopy*. Wiley, 1988.

CURRICULUM VITAE

PERSONAL INFORMATION

Surname, Name: Esin, Yunus Emre
Nationality: Turkish (TC)
Date and Place of Birth: 21.07.1984, Turhal / TOKAT
Marital Status: Married

EDUCATION

Degree	Institution	Year of Graduation
Ph.D.	Department of Computer Engineering, METU	2017
M.Sc.	Department of Computer Engineering, METU	2009
B.S.	Department of Computer Engineering, METU	2007
High School	Turhal Anadolu Lisesi	2002

PROFESSIONAL EXPERIENCE

Year	Place	Enrollment
2014-Present	SGBT/ HAVELSAN	R&D Team Leader
2007-2014	Corporate Technology / SIEMENS	Senior Software Engineer

PUBLICATIONS

International Conference Publications

Esin, Y.E, Alan, O and Alpaslan, F.N. Improvement on Corpus-Based Word Similarity Using Vector Space Models. Computer and Information Sciences, 2009. ISCIS 2009. 24th International Symposium on Computer and Information Sciences

Ozturk, S., Artan, Y., Esin, Y. E., Yaman, M. and Erdem, A. (2015, July). Semi-supervised gas detection in hyperspectral imaging. In Geoscience and Remote Sensing Symposium (IGARSS), 2015 IEEE International (pp. 469-472). IEEE.

Ozturk, S., Esin, Y. E. and Artan, Y. (2015, October). Object detection in rural areas using hyperspectral imaging. In SPIE Remote Sensing (pp. 96432M-96432M). International Society for Optics and Photonics.

B Demirel, Ö Özdil, YE Esin. Hyperspectral image segmentation based on spatial model 2016 24th Signal Processing and Communication Application Conference

Ş Öztürk, Y Artan, YE Esin. Ethene and CO_2 gas detection in hyperspectral imagery 2016 24th Signal Processing and Communication Application Conference

MS Thesis

Esin, Y.E. Improvement of Corpus-Based Semantic Word Similarity Using Vector Space Model, METU-CENG, July. 2009